Development of Controller for the Post-Catalyst Oxygen Sensor on EcoCAR Vehicle

Undergraduate Honors Thesis

Presented in Partial Fulfillment of the Requirements for Graduation with Distinction at The Ohio State University

By

Katherine M. Bovee

* * * * *

The Ohio State University

2010

Defense Committee:

Professor Giorgio Rizzoni, Advisor

Dr. Shawn Midlam-Mohler, Advisor

Professor Yann Guezennec

ABSTRACT

Increasingly stringent regulations on emissions require automobile manufacturers to find new ways to reduce the emissions produced by their vehicles. Competitions like EcoCAR challenge engineering students to modify a production vehicle to reduce the vehicle's energy consumption and tailpipe emissions, while maintaining standard vehicle performance. The purpose of this project is to develop a strategy to reduce the emissions produced by the EcoCAR vehicle, using the catalytic converter and post-catalyst oxygen sensor in the vehicle's exhaust system. A proportional-integral controller is used with the post-catalyst oxygen sensor, to keep the engine operating as close to stoichiometry as possible. The following research describes how a phenomenological model of a catalytic converter was developed and validated. The model of the catalytic converter was then used in a simulation of the post-catalyst oxygen sensor controller, to determine the most effective proportional and integral gains for the controller. The post-catalyst oxygen sensor controller was then integrated into the EcoCAR's overall engine controller, so emissions testing could be performed. The results of the emissions test showed the EcoCAR vehicle should meet the Environmental Protection Agencies Tier 2, Bin 5 emission regulations, when the EcoCAR vehicle is operating in series mode.

ACKNOWLEDGMENTS

I would like to thank Dr. Giorgio Rizzoni for the chance to participate in this undergraduate research project. I would especially like to thank Dr. Shawn Midlam-Mohler, for all the guidance he has given me during this research project. I would like to thank Beth Bezaire for all her help learning about catalytic converters and the EcoCAR team in general. I would also like to thank Brad Cooley, Josh Supplee and Ryan Everett for helping me learn how to run the EcoCAR engine and figure out the engine controller code. Finally, I would like to acknowledge the financial support I received from the National Science Foundation, under the grant CMMI0928518, “A System Dynamics Modeling Methodology to Predict Transient Phenomena in Compressible Fluid Flow Systems.”

TABLE OF CONTENTS

LIST OF FIGURES

Figure Page

LIST OF TABLES

CHAPTER 1: INTRODUCTION

1.1 Introduction

Throughout the past century, the internal combustion engine has revolutionized the way people travel. The engine in Ford's 1908 Model-T made travel more accessible to middle-class Americans, while today's engines make hybrid vehicles and high performance sports cars possible. In recent years, both governments and consumers have become increasingly concerned about the effect automobile use has on climate change and global warming. The automotive industry has responded to the concerns by looking for new technologies to make internal combustion engines more fuel-efficient and produce fewer emissions.

To encourage research into more environmentally friendly vehicles, the U.S. Department of Energy, General Motors and other industry leaders sponsor the EcoCAR Challenge competition. In the EcoCAR competition, teams of students modify a Saturn Vue to reduce the vehicle's energy consumption and emissions while maintaining the vehicle's original utility, safety and performance. To accomplish the goals of the competition, student teams design, build and integrate advanced propulsion technologies

into the vehicle. The advanced propulsion technologies include electric, hybrid, plug-in hybrid and fuel cell powertrains.

The Ohio State EcoCAR team decided to use a plug-in hybrid propulsion system in their vehicle. The vehicle uses an internal combustion engine to provide power to the two electric motors responsible for moving the vehicle. The engine is also capable of storing energy inside the vehicle's batteries for later use. The internal combustion engine chosen for the vehicle is a 1.8L Honda four-cylinder engine in the compressed natural gas (CNG) configuration.

The EcoCAR team chose to use a CNG engine, because CNG has a higher octane rating than regular gasoline. A fuel with a higher octane rating allows an engine to have a higher compression ratio. The higher the compression ratio of an internal combustion engine, the greater the efficiency and fuel economy of the vehicle. Instead of using compressed natural gas for fuel, the OSU team will be using E85, which is a mixture of 85% ethanol and 15% gasoline by volume. E85 has a similar octane rating to CNG, and has up to 40-50% less hydrocarbon and nitrogen oxides emissions than regular gasoline (Dai, Cheemalamarri, Curtis, Boussarsar and Morton, 2003).

One of the evaluation criteria for the EcoCAR vehicle during competitions is the amount of emissions it produces while in operation. The emissions include hydrocarbons (THC), carbon monoxide (CO), nitrogen oxides (NO_x) and particulates. To reduce the amount of emissions produced by the vehicle, a three-way catalytic converter is used in the vehicle's exhaust system. A catalytic converter is able to take the gaseous emissions

exiting the engine and convert them to carbon dioxide and water. To keep the catalytic converter operating at its peak efficiency, oxygen sensors are placed before and after the catalyst to monitor the catalyst's state. A controller is then used with the oxygen sensors to make small changes in engine's operation in order to keep the catalyst operating at peak efficiency at all times.

1.2 Motivation

As emissions standards become more stringent and petroleum prices continue to increase, alternative fuels like E85 will become a more viable option for powering vehicles. Although E85 produces fewer emissions than regular gasoline, a catalytic converter is still needed for E85 vehicles to meet emission standards. Vehicles using E85 also need oxygen sensors that are used with a robust controller to monitor the state of the catalyst, in order to keep the catalyst operating at peak efficiency at all times. The knowledge gained from the EcoCAR project, as well as from research presented in this thesis, could be used in the future to produce more environmentally friendly vehicles.

1.3 Project Objective

The goal of this research is to minimize the emissions of the EcoCAR vehicle. Therefore, a controller is required to monitor the state of the catalytic converter with oxygen sensors, and make slight changes in the engine's operation to keep the catalyst operating at peak efficiency. The first step to creating the controller is to create a model of the catalytic converter's behavior, using data from the oxygen sensors located before

and after the catalyst. The model can then be used in a simulation environment to create and optimize a controller for the catalytic converter. The next step is to integrate the catalyst's controller into the overall engine controller code. The final step is using an emissions analyzer to measure the amount of emissions leaving the catalytic converter and to make final changes in the controller design to minimize emissions.

CHAPTER 2: LITERATURE REVIEW

2.1 Engine Operating Conditions

The goal of designing a controller for the post catalyst oxygen sensor is to keep the engine operating near a stoichiometric ratio of fuel/air and recover from disturbances to the fuel/air ratio. The fuel/air ratio of the engine is the rate of fuel entering the engine divided by the rate of air entering the engine, as shown in Equation 2.1. The inverse of Equation 2.1 gives the air/fuel ratio of the engine, as shown in Equation 2.2. The stoichiometric air/fuel ratio of an engine operating with E85 fuel is 9.87. The equivalence ratio is another way of expressing the air/fuel ratio of the engine. Equation 2.3 states the equivalence ratio of an engine is the actual fuel/air ratio of the engine divided by the stoichiometric fuel/air ratio of the engine. If an engine is operating rich, it has an equivalence ratio greater than one, and if an engine is operating lean, it has an equivalence ratio of less than one. The inverse of Equation 2.3 gives the relative air/fuel ratio of an engine, as shown in Equation 2.4.

$$(F/A) = \frac{\dot{m}_f}{\dot{m}_a} \qquad \text{Equation 2.1}$$

$$(A/F) = \frac{\dot{m}_a}{\dot{m}_f} \qquad \text{Equation 2.2}$$

$$\phi = \frac{(F/A)_{actual}}{(F/A)_s} \qquad \text{Equation 2.3}$$

$$\lambda = \frac{(A/F)_{actual}}{(A/F)_s} \qquad \text{Equation 2.4}$$

2.2 Background on Catalytic Converters

The catalytic converter in an automobile takes the unwanted emissions in the exhaust gases, such as hydrocarbons (HC), carbon monoxides (CO), and nitrogen oxides (NO_x), and turns them into less harmful compounds like water (H_2O), carbon dioxide (CO_2) and nitrogen (N_2). Oxidation reactions convert the HC and CO emissions to H_2O and CO_2. Reduction reactions react the NO_x emissions with CO, HC and H_2 molecules in the exhaust gases to form H_2O, CO_2 and N_2. A three-way catalyst (TWC) is able to oxidize the hydrocarbon and carbon monoxide emissions while simultaneously reducing the NO_x emissions.

The structure of a catalytic converter consists of a ceramic substrate, a washcoat containing the active catalyst material, and a metal container, as shown in Figure 2.1. The substrate is made up of a ceramic honeycomb structure with square cross-sectional passageways. Generally, the sides of each passageway in the range of 1 mm long. The

washcoat is a porous material applied to the ceramic substrate. The washcoat contains the active catalyst material, which is some combination of platinum (Pt), palladium (Pd) and rhodium (Rh). The type of catalyst material impregnated into the washcoat depends on the type of pollutants the catalytic converter will catalyze. Both platinum and palladium are effective at oxidizing HC and CO, while rhodium is mainly used to reduce NO_x (Heywood, 1988). In order to mount the catalytic converter to the exhaust system, the ceramic substrate is inserted into a metal container called a can (Schmidt, Franz and Merdes, 2002).

A three-way catalyst has the highest conversion efficiency for removing NO_x, CO and HC from the exhaust gases when the engine is operating near its stoichiometric air/fuel ratio. Figure 2.2 shows the conversion efficiencies for NO_x, HC and CO for a catalyst in a gasoline engine. Although the engine used for the experiments in this thesis

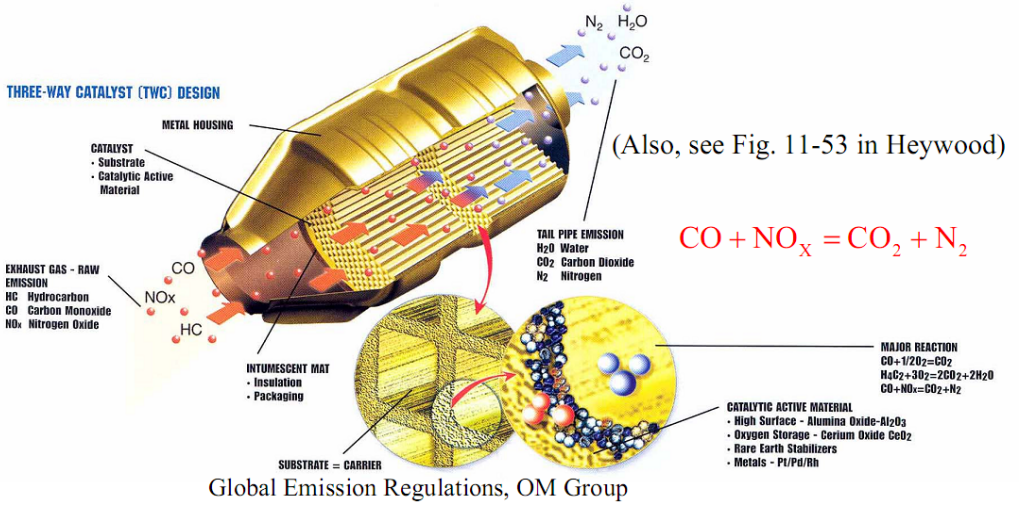

Figure 2.1: Structure of Three-Way Catalyst (Selamet, 2009)

will operate on E85 instead of gasoline, catalytic converters working with E85 still exhibit the same trends as those shown in Figure 2.2. The figure shows that if the air/fuel ratio of the engine changes from stoichiometry by more then 0.1, the conversion efficiencies for HC, CO and NO_x drop significantly. If the engine runs slightly lean, the excess oxygen in the exhaust gases oxidizes all the HC and CO, but most of the NO_x is not reduced. If the engine runs slightly rich, the lack of oxygen in the exhaust gases allows all the NO_x to be reduced, but most of the HC and CO cannot be oxidized (Heywood, 1988).

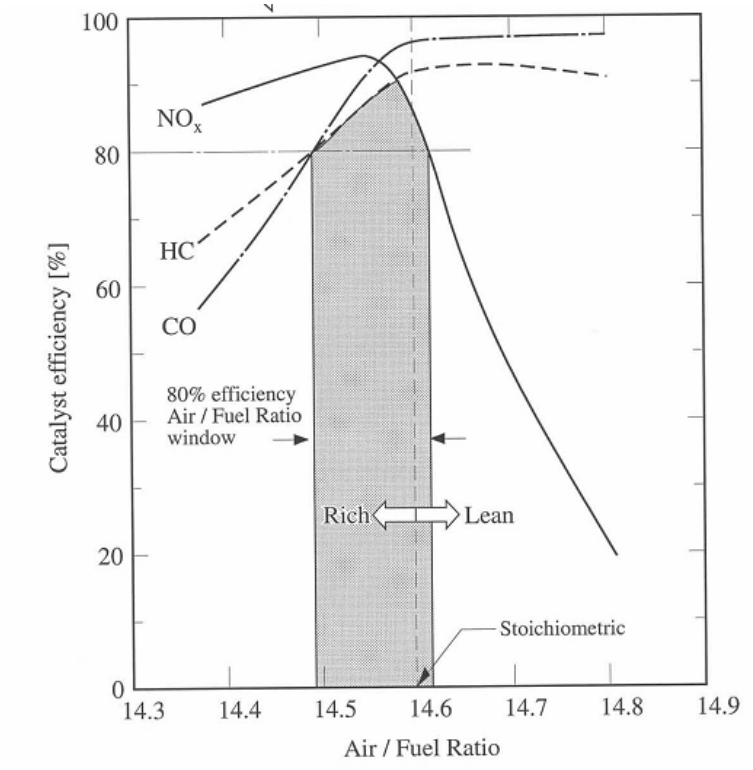

Figure 2.2: Catalyst Conversion Efficiency as a Function of Air/Fuel Ratio in Gasoline Engines (Heywood, 1988)

The catalyst can maintain a high conversion efficiency despite disturbances in the engine's air/fuel ratio, due to the oxygen storage capacity of the catalyst. The precious metals coating the catalyst substrate are capable of reacting with the excess oxygen in the exhaust gases. The chemical reactions allow the catalyst to store the oxygen when the engine runs lean, and release the oxygen when the engine runs rich. Therefore, the oxygen storage capacity of the catalyst allows the catalyst to act as a buffer to the air/fuel ratio of the exhaust gases exiting the engine. Figure 2.3 shows measurements made by the pre and post-catalyst oxygen sensors, which measure the equivalence ratio of the exhaust gases. When the engine starts to run lean, the catalyst starts to absorb oxygen and keeps the exhaust gases inside the catalyst at stoichiometry, creating the first plateau. The gases inside the catalyst only become lean once the catalyst has absorbed as much oxygen as it can. Then when the engine starts to run rich again, the catalyst releases some of the oxygen inside of it to keep the exhaust gases at stoichiometry and create the second plateau shown in Figure 2.3. Once the catalyst has depleted its store of oxygen, the gases passing through the catalyst become rich (Brandt, Wang and Grizzle, 2000).

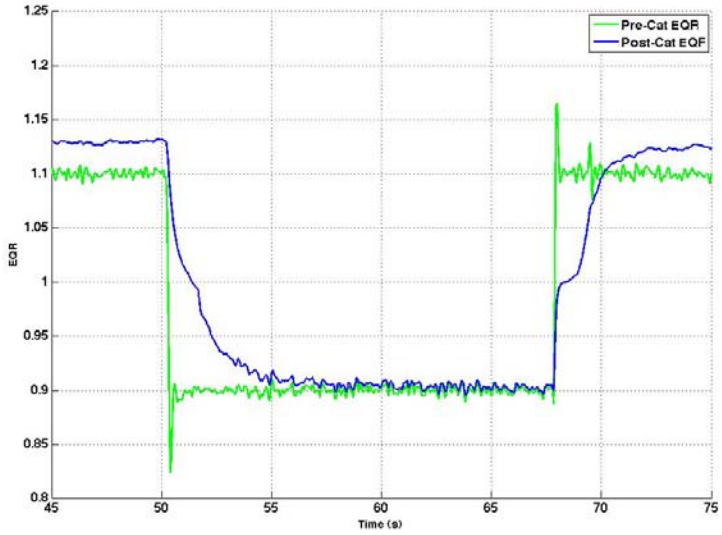

Figure 2.3: Oxygen Storage Characteristics of Catalysts

Another factor affecting the conversion efficiency of the catalyst is the temperature of the catalyst's substrate, as shown in Figure 2.4. When the catalyst's temperature is below 300^{o}C, the reaction rates for the oxidation and reduction reactions are too slow to catalyze any of the emissions in the exhaust gases. Therefore, the catalyst has very poor conversion efficiencies for HC, CO and NO_x when its internal temperature is less than 300^{o}C (Heywood, 1988).

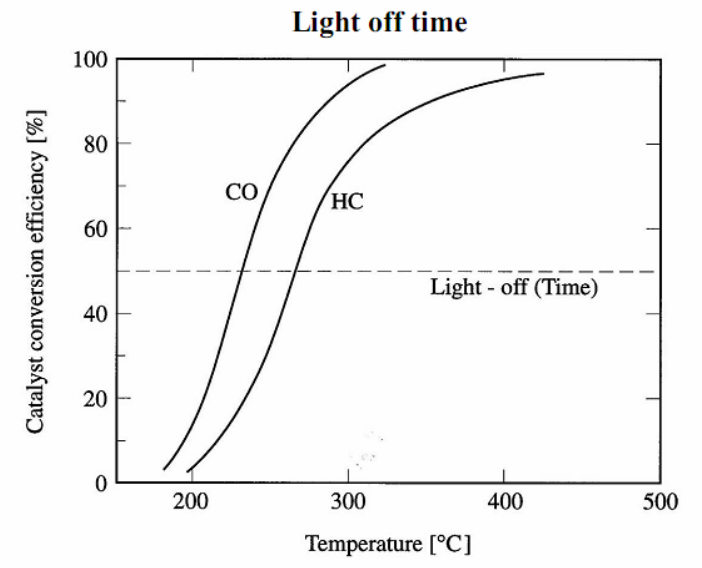

Figure 2.4: Catalyst Efficiency as a Function of Temperature (Heywood, 1988)

The catalyst's conversion efficiency also deteriorates as the catalyst ages, due to effects of poisoning and sintering. Poisoning is when the chemical reactions inside the catalyst are hindered by prolonged contact with interfering elements. The interfering elements either interact chemically with the active catalyst material or physically block the reaction sites in the catalyst. The main interfering elements are lead in antiknock agents and phosphorus in oil additives. Sintering occurs at high temperatures and involves the migration of active sites, thus decreasing the surface area for chemical reactions to take place (Heywood, 1988).

2.3 Oxygen Sensors

The pre and post-catalyst oxygen sensors in an exhaust system are critical to regulating the air/fuel ratio of the engine. A diagram of an oxygen sensor is shown in Figure 2.5. The oxygen sensor is made up of a solid electrolyte that current is carried

through by oxygen ions. A ceramic electrolyte separates two platinum electrodes, which hold exhaust gases and atmospheric air. The difference in oxygen partial pressures between the two platinum electrode chambers causes the oxygen ions to carry current between the chambers (Midlam-Mohler, 2010). The two main types of oxygen sensors are the universal exhaust gas oxygen (UEGO) sensors and the switching-type (EGO) sensor. The UEGO sensor measures the air/fuel ratio of the engine. The EGO sensor mainly indicates if the engine is operating lean or rich.

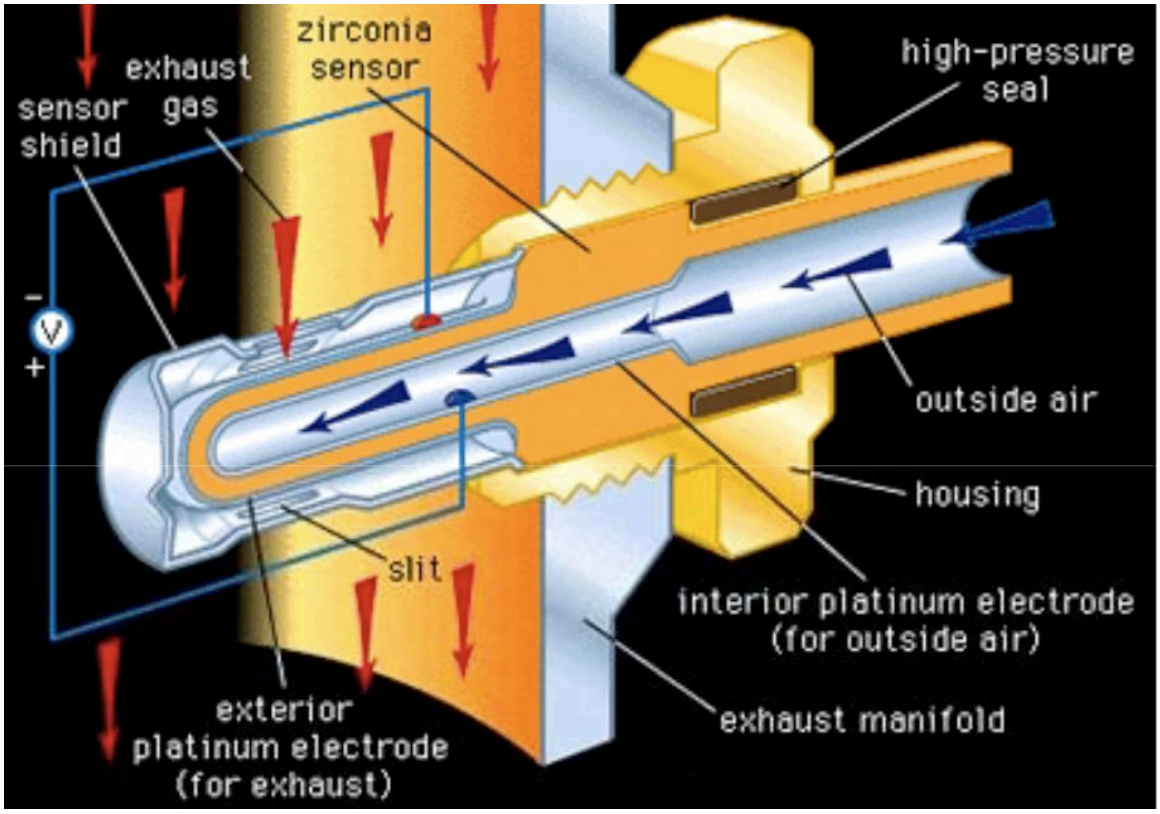

Figure 2.5: Structure of Oxygen Sensors (ME 631 Lecture 7, Winter 2010)

One problem with the oxygen sensors is they measure the air/fuel ratio of the exhaust gases at the sensor's surface, instead of the actual air/fuel ratio of the exhaust gases. Before the oxygen sensor can measure the air/fuel ratio, the molecules in the exhaust gases must first diffuse through a porous ceramic layer before they reach the platinum electrode, as shown in Figure 2.6. Smaller particles like hydrogen tend to have a higher diffusion rate than heavier species like hydrocarbons. Therefore, different exhaust gas species have different concentrations at the sensor surface, which causes the oxygen sensor to inaccurately measure air/fuel ratios. Figure 2.7 and Figure 2.8 shows the voltage output of an oxygen sensor as the gases passing through it are changed from rich to lean. The chemical composition of each gas has different amounts of hydrogen, hydrocarbons and other particles, in order measure the effect each particle has on the relative air/fuel ratio measured by the oxygen sensor. The results of the experiment show species like hydrogen with lower molecular weights cause a lean shift in the measured relative air/fuel ratio, while species like hydrocarbons with higher molecular weights cause a rich shift in the measured relative air/fuel ratio (Buglass, Morgan and Grauper, 1998).

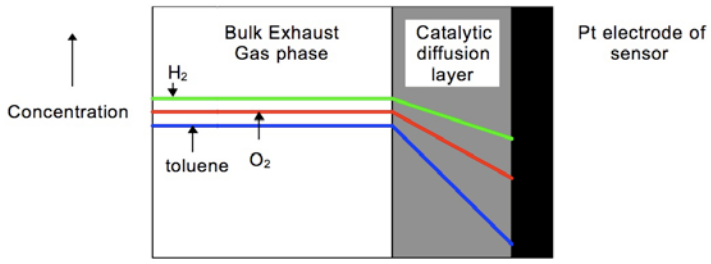

Figure 2.6: Schematic of Relative Diffusion Rates of Exhaust Gas Components (Buglass, Morgan and Grauper, 1998)

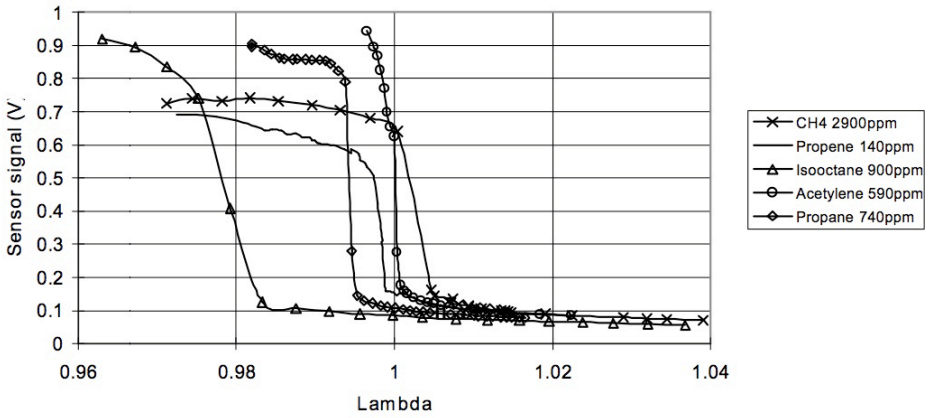

Figure 2.7: Lean Relative Air/Fuel Ratio Shift due to Particles in the Exhaust Gases (Buglass, Morgan and Grauper, 1998)

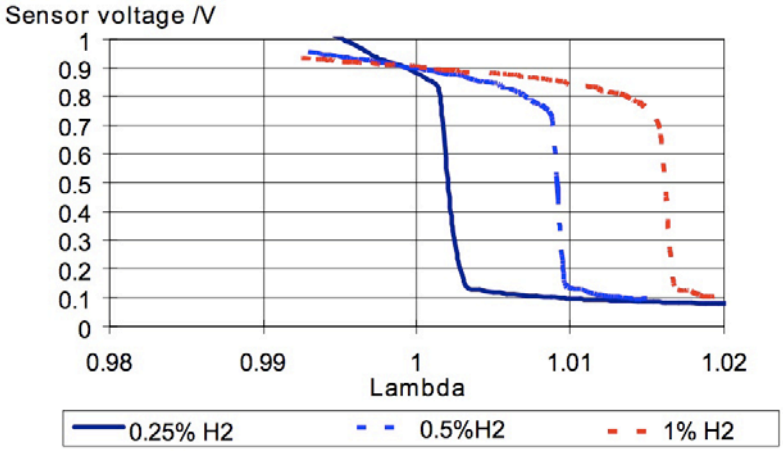

Figure 2.8: Rich Relative Air/Fuel Ratio Shift due to Particles in the Exhaust Gases (Buglass, Morgan and Grauper, 1998)

2.4 Catalyst Models

Traditionally, catalytic converter models have been based on nonlinear partial differential equations. The differential equation models are complex and hard to work with, due to the difficultly in deriving numerical values for different model parameters. Many differential equation models are also unable to calculate reliable steady-state

characteristics of a catalyst. An alternative way of modeling a catalytic converter is a dynamic model based on the engine's air/fuel ratio.

One dynamic model developed by Erich Brandt, Yanying Wang and Jesse Grizzle is shown in Figure 2.9. There are three parts to the model: the heat transfer element, the conversion efficiency of the catalyst and the oxygen storage element. The model works by calculating the air/fuel ratio of the gases leaving the catalyst by using the oxygen storage model, the air/fuel ratio of the gases entering the catalyst and the engine's mass airflow. The internal temperature of the catalyst is then used to adjust the catalyst's conversion efficiency map. The tailpipe air/fuel ratio and the modified efficiency maps are then used to estimate the catalyst conversion efficiencies for NO_x, HC and CO. The conversion efficiencies are then used with the concentrations of emissions in the exhaust gases before the catalyst to calculate the total emissions exiting the catalyst.

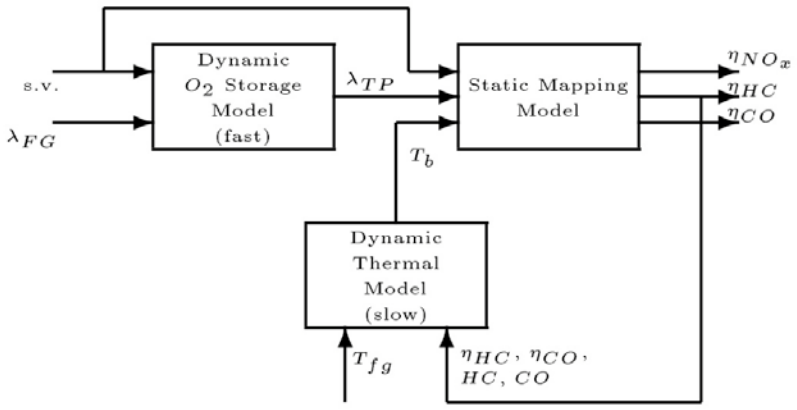

Figure 2.9: Structure of Three-Way Catalyst Model (Brandtl, Wang and Grizzle)

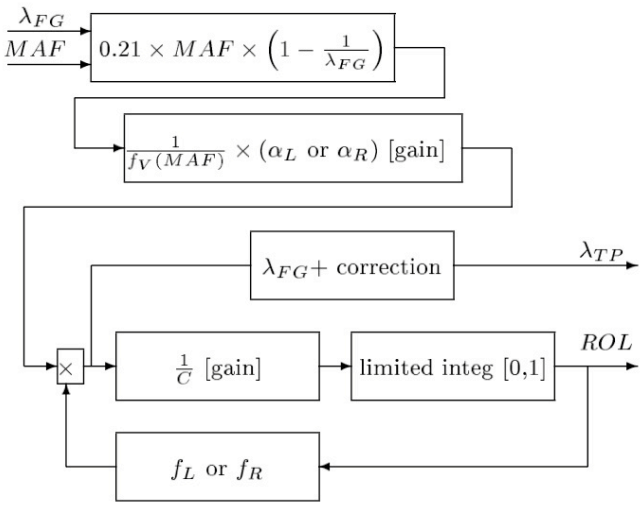

Figure 2.10: Structure of Oxygen Storage Model (Brandtl, Wang and Grizzle)

The heat transfer model estimates the temperature of the catalyst. During cold start, the temperature of the catalyst is dependent on the heat transfer from the exhaust gases. Once the catalyst is warmed up, its temperature is dependent on the chemical reactions occurring between the catalyst and exhaust gases. The conversion efficiency model is based on experimental data taken at steady state, with the conversion efficiencies correlated with the estimated air/fuel ratio of the exhaust gases exiting the catalyst.

The oxygen storage model shown in Figure 2.10 estimates the relative level of oxygen (ROL) stored in the catalyst and calculates the air/fuel ratio of the gases exiting the catalyst. The model first calculates the net amount of free oxygen in the exhaust gases with the engine's mass airflow and the air/fuel ratio of the gases entering the catalyst, as shown in the following equations.

$$\dot{m}_{O2,net} = 0.21 \times MAF \times \left(1 - \frac{1}{\lambda_{FG}}\right) \qquad \text{Equation 2.5}$$

$$\rho(\lambda_{FG}, \Theta) = \begin{cases} \alpha_L f_L(\Theta) & \lambda_{FG} > 1 \\ \alpha_R f_R(\Theta) & \lambda_{FG} < 1 \end{cases} \qquad \text{Equation 2.6}$$

In Equation 2.5, $\dot{m}_{O2,net}$ is the net amount of free oxygen, *MAF* is the engine's mass airflow and λ_{FG} is the relative air/fuel ratio of the gases entering the catalyst. The model then calculates the rate the catalyst is absorbing or releasing oxygen using the plots in Figure 2.11 and Equation 2.6. In Equation 2.6, ρ is the rate of oxygen absorption or release, f_L and f_R are the relative oxygen absorption and release rates and α_L and α_R are experimentally derived constants. The relative oxygen absorption and release rates are found in Figure 2.11 using the catalyst's current relative oxygen level.

The oxygen rate of change inside the catalyst is found by multiplying the net amount of free oxygen in the exhaust gases with the oxygen absorption/release rate, and

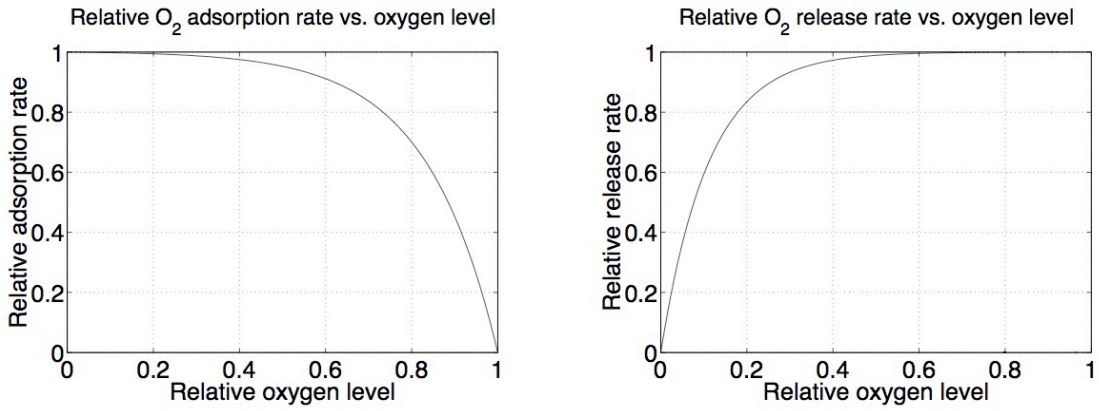

Figure 2.11: Relative Oxygen Absorption and Release Rates as a Function of Relative Oxygen Level (Brandtl, Wang and Grizzle)

then dividing the result by the oxygen storage capacity of the catalyst, as shown in the following equation.

$$\dot{\Theta} = \begin{cases} \frac{1}{C(MAF)} \times \rho(\lambda_{FG}, \Theta) \times \dot{m}_{O2,net} & 0 \le \Theta \le 1 \\ 0 & otherwise \end{cases} \qquad \text{Equation 2.7}$$

In Equation 2.7, $\dot{\Theta}$ is the rate of change of oxygen inside the catalyst and *C* is the oxygen storage capacity of the catalyst that is dependent on the engine's mass airflow. The result of Equation 2.7 is then integrated to get the relative oxygen level inside the catalyst. The air/fuel ratio of the gases exiting the catalyst are calculated in Equation 2.8, where λ_{TP} is the relative air/fuel ratio of the gases exiting the catalyst, λ_{FG} is the relative air/fuel ratio of the gases entering the catalyst and ρ is the rate of change of oxygen inside the catalyst.

$$\lambda_{TP} = \lambda_{FG} - \rho(\lambda_{FG}, \Theta) \times (\lambda_{FG} - 1) \qquad \text{Equation 2.8}$$

The dynamic catalyst model developed by Brandt, Wang and Grizzle models the fundamental behavior of the catalytic converter, but it does have some problems.

2.5 Oxygen Sensor Controllers

The oxygen sensors in a vehicle's exhaust system measure the air/fuel ratio of the exhaust gases. The measurements allow the engine controller to adjust the amount of fuel injected into the engine cylinders, in order to keep the air/fuel ratio of the exhaust gases at stoichiometry. The closer the air/fuel ratio of the exhaust gases are to stoichiometry, the higher the catalyst's efficiency at converting emissions to water, nitrogen and carbon dioxide.

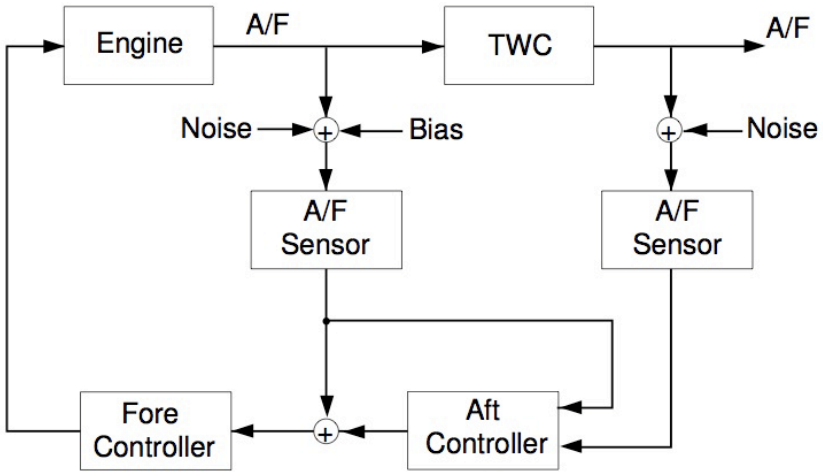

Figure 2.12: Duel-UEGO Sensor Controller Structure (Fiengo, Grizzle, Cook and Karnik, 2005)

One method of keeping the air/fuel ratio of the gases inside the catalyst at stoichiometry is to use two oxygen sensors in the exhaust system: one before the catalyst and one after the catalyst. Figure 2.12 is a diagram of how the two oxygen sensors and their controllers can be used to manage the air/fuel ratio of the exhaust gases. The oxygen sensor behind the catalyst is used with the aft proportional controller to adjust the set point of the fore controller. The set point adjustments made by the aft controller result in small changes in the engine's air/fuel ratio. The aft controller also estimates the bias, which is the difference in the air/fuel ratios of the exhaust gases before and after the catalyst (Fiengo, Grizzle, Cook and Karnik, 2005).

The oxygen sensor in front of the catalyst is used with the fore proportional-integral (PI) controller to make large changes in the engine's air/fuel ratio. The fore controller first subtracts the bias calculated by the aft controller from the air/fuel ratio

measured by the fore oxygen sensor. The resulting signal is then compared to the set point calculated by the aft controller, and the error between the two signals is put through the proportional-integral part of the controller. The output of the fore controller is then used to adjust the air/fuel ratio of the engine (Fiengo, Grizzle, Cook and Karnik, 2005).

CHAPTER 3: EXPERIMENTAL DESCRIPTION

The research described in this thesis was performed at the Center for Automotive Research at The Ohio State University. The 1.8L Honda four-cylinder engine is connected to a four-quadrant 200 hp DC dynamometer, which is used to control engine speed. A variety of sensors are mounted on the engine and connected to the engine's Woodward ECU and the ETAS data acquisition systems. An Emitec electrically heated three-way catalyst is also mounted in the engine's exhaust system. The emissions from the engine are measured with a Horiba MEXA 7500 emissions analyzer. The Horiba MEXA 7500 is capable of measuring total hydrocarbons (THC), carbon monoxide (CO), nitrogen oxides (NO_x), carbon dioxide (CO_2), oxygen (O_2) and hydrogen (H_2).

3.1 Honda Engine

The 1.8L Honda four-cylinder engine has a variable-length air intake manifold and variable valve lift timing. Figure 3.1 shows the variable-length air intake manifold. At low engine speeds the bypass valve is closed in order to lengthen the air intake manifold. The bypass valve is then opened at engine speeds of 5000 rpm and higher to shorten the air intake manifold and increase the engine's torque output, as shown in Figure 3.2 (Watanabe, Nakajima, Goto and Matsunaga, 2007). When the engine is put

inside the EcoCAR vehicle, it operates within the 1000-3000 rpm range. Therefore, the bypass valve was always closed for this research project.

The Honda engine is capable of variable valve lift timing, which is done using the engine's high-output and delayed closure cams. Figure 3.3 shows the high-output cam produces a larger amount of torque than the delayed closure cam. The delayed close cam

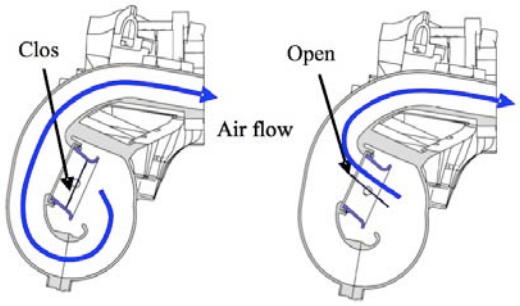

Figure 3.1: Diagram of Honda Engine Variable-Length Air Intake Manifold (Watanabe, Nakajima, Goto and Matsunaga, 2007)

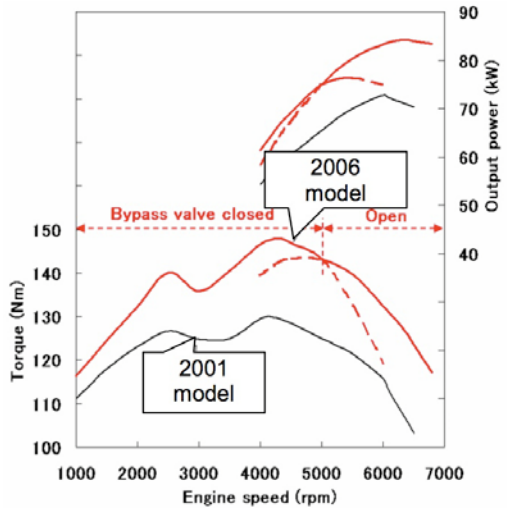

Figure 3.2: Torque and Power Output of Variable-Length Air Intake Manifold (Watanabe, Nakajima, Goto and Matsunaga, 2007)

is used to reduce pumping losses and improve fuel economy, by causing the intake valve to close later in the compression stroke (Watanabe, Nakajima, Goto and Matsunaga, 2007). However, previous research done by the EcoCAR team indicated the high-output cam should be used in the EcoCAR vehicle at all times (Davis, 2010). The EcoCAR vehicle is a hybrid, so the vehicle is able to use its batteries to either store extra power from the engine, or release electricity if the engine is not producing enough power. Therefore, the engine is always able to operate in the high manifold air pressure region, where pumping losses are already reduced and the delayed closure cam is unnecessary. For the research done in this thesis, the high-output cam was always used.

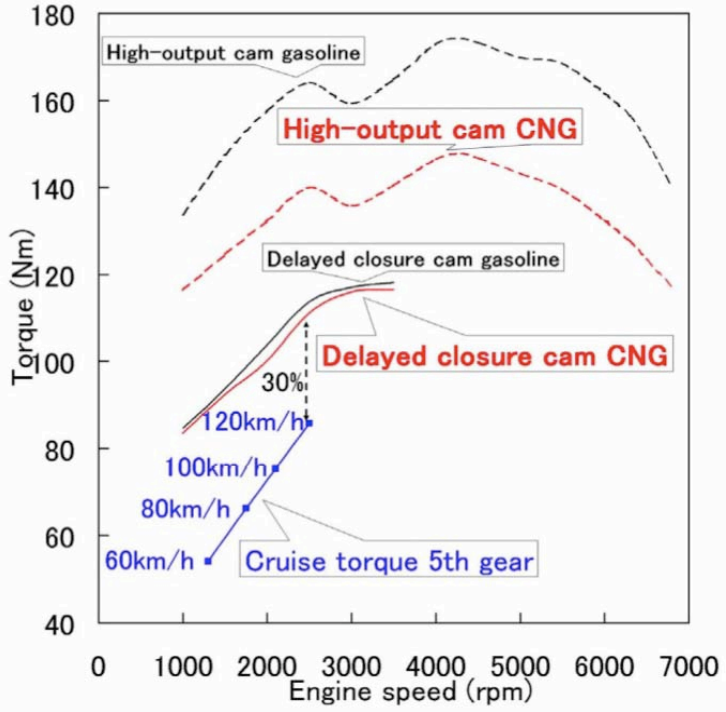

Figure 3.3: Comparison of CNG and Gasoline Engine Torque Output with Variable Valve Lift Timing (Watanabe, Nakajima, Goto and Matsunaga, 2007)

3.2 Emitec Catalytic Converter

The catalytic converter in the EcoCAR vehicle is an Emitec Emicat Series 6d electrically heated three-way catalyst. In an electrically heated catalyst, electricity is run through the first portion of the catalyst substrate that heats up the exhaust gases passing through it. The heated exhaust gases then pass through the rest of the catalyst substrate that hold the active catalytic material, causing the catalyst to heat up faster. Figure 3.4 shows the total amount of hydrocarbons produced during operation is reduced when the catalyst is able to heat up faster. The catalytic converter is also close-coupled to the Honda engine, to further reduce the time the catalyst takes to warm up when the engine is turned on.

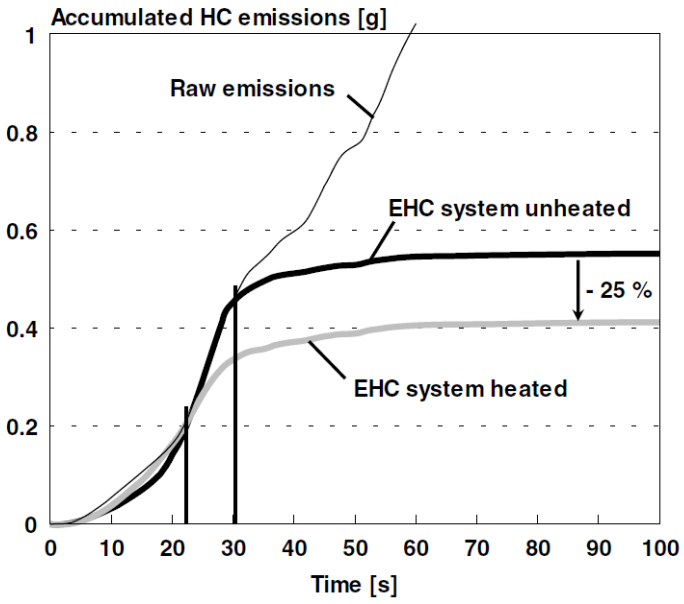

Figure 3.4: Effectiveness of Electrically Heated Catalyst in Reducing Hydrocarbon Emissions (Holy, Bruck and Hirth, 2000)

3.3 Engine Instrumentation

The Honda engine is equipped with a variety of sensors, which are listed in Table 3.1. Figure 3.5, Figure 3.6 and Figure 3.7 show the locations of the sensors used specifically for the research in this thesis. The sensors are either directly connected to the engine's Woodward ECU or are connected to an external data acquisition system. The Horbia ports before and after the catalyst, which are listed as numbers 21 and 24 in Table 3.1, are used to connect the Horiba MEXA 7500's sample lines to the engine's exhaust system. The engine is also equipped with a water-cooled cooling tower, which uses its own built in thermostat to regulate the coolant temperature of the engine.

The knock sensor listed as number 8 in Table 3.1 is a simple copper tube with a funnel on one end. The other end of the knock sensor is attached to the engine block where the original Honda piezoelectric knock sensor was located. The funnel of the copper pipe knock sensor is fed into the engine control room, so the person operating the engine can hear when the engine starts to knock.

Table 3.1: List of Engine Sensors

No.	Sensors / Ports	Data Acquisition System
1	Barometric Pressure	ETAS
2	Camshaft Position Sensor	Woodward ECU
3	Crank Encoder	ETAS
4	Crankshaft Position Sensor	Woodward ECU
5	EGR (Exhaust Gas Recirculation) Valve	Woodward ECU
6	Engine Coolant Flow Rate Sensor	ETAS
7	Engine Coolant Temperature Sensor	Woodward ECU
8	Engine Knock Sensor	N/A
9	Engine Oil Pressure Sensor	Woodward ECU
10	Ethanol Concentration Sensor	Woodward ECU
11	Fuel Level Sensor	Woodward ECU
12	Fuel Rail Pressure Sensor	Woodward ECU
13	Fuel Tank Pressure Sensor	Woodward ECU
14	Intake Air Temperature Sensor	Woodward ECU
15	Intake Manifold Thermocouple	Woodward ECU
16	MAF (Mass Air Flow) Sensor	Woodward ECU
17	MAP (Manifold Air Pressure) Sensor	Woodward ECU
18	Post-Catalyst EGO Sensor	Woodward ECU
19	Post-Catalyst Exhaust RTD	Woodward ECU
20	Post-Catalyst Horiba Port	Horiba
21	Post-Catalyst UEGO Sensor	ETAS
22	Pre-Catalyst Exhaust RTD	Woodward ECU
23	Pre-Catalyst Horiba Port	Horiba
24	Pre-Catalyst UEGO Sensor	Woodward ECU
25	Throttle Position Sensor	Woodward ECU

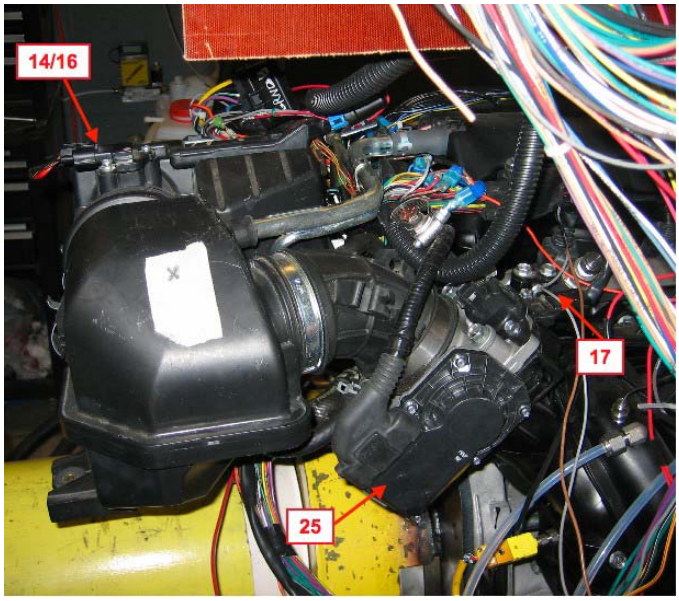

Figure 3.5: Engine Sensors Locations on Front of Engine

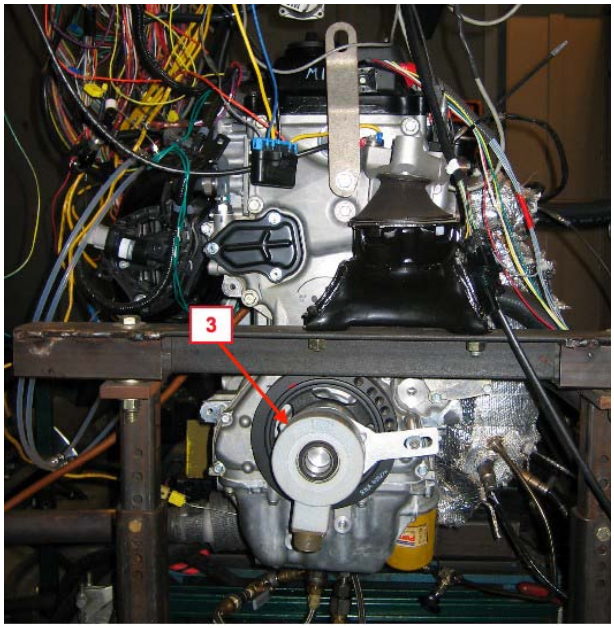

Figure 3.6: Engine Sensor Locations on Side of Engine

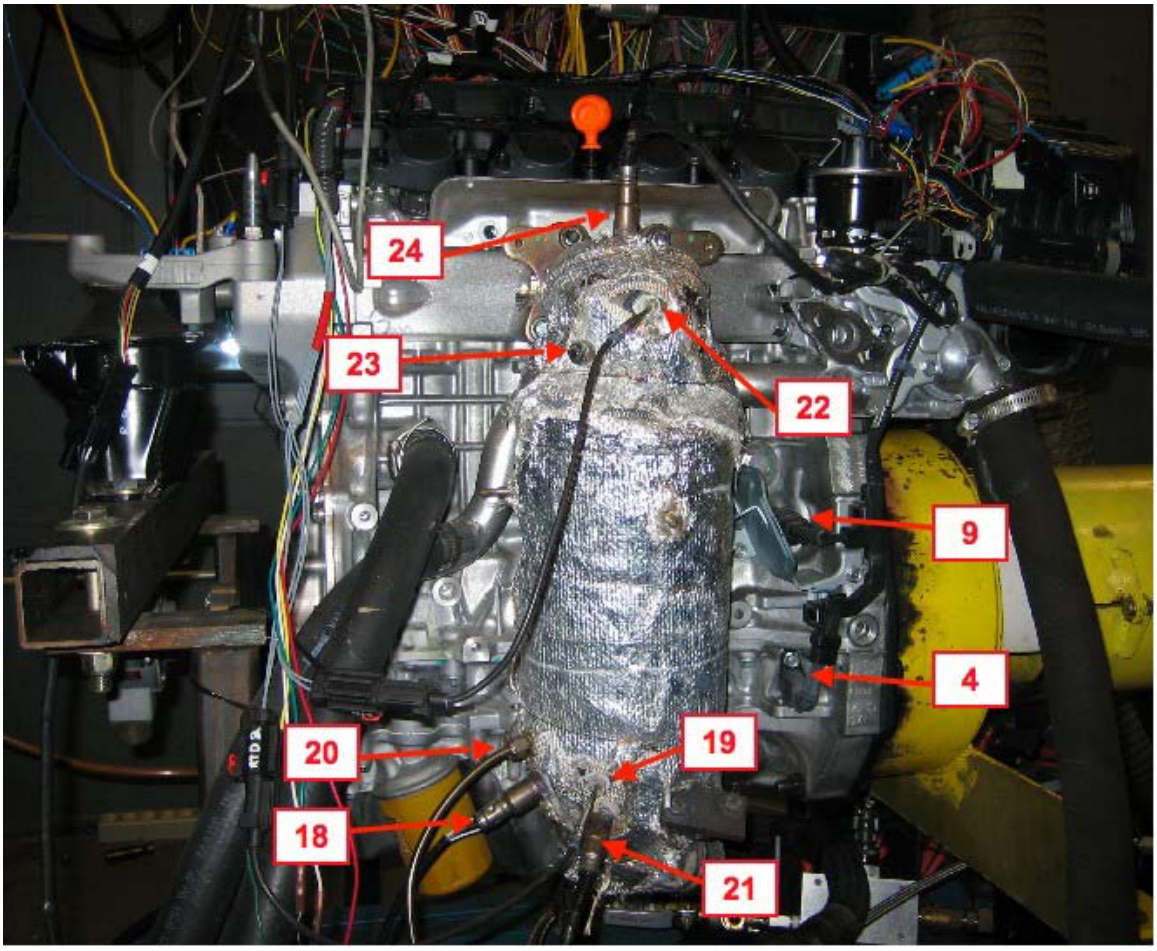

Figure 3.7: Engine Sensor Locations on Back of Engine

The sensors used to directly monitor the state of the catalyst are the pre-catalyst UEGO sensor, post-catalyst UEGO sensor and post-catalyst EGO sensor. The UEGO sensors can directly measure the equivalence ratio of the exhaust gases, while the EGO sensor is only able to determine if the exhaust gases are lean or rich of stoichiometry. The post-catalyst UEGO sensor is only for research purposes, since it will not be integrated into the EcoCAR vehicle's exhaust system. The pre and post-catalyst exhaust RTD sensors are also used to monitor the temperature of the exhaust gases before and after the catalyst. The mass airflow (MAF) sensor located in intake manifold is also important to

the catalytic converter, since the catalyst's behavior is dependent on the amount of air flowing through the engine.

3.4 Data Acquisition System

Several data acquisitions systems are used to read the data signals coming from the sensors on the engine. The first system consists of four ETAS modulus, which can read signals from thermocouples and other sensors that use BNC cables. Each ETAS module is used for sensors that were not part of the Honda engine's original wiring harness. The ETAS modules include the ETAS ES410 that has 8 analog channels, the ETAS ES411 that has 4 analog channels with a sensor supply voltage, and two ETAS ES420 that have 8 thermocouple channels each. An ETAS LA4 Lambda Meter signal conditioner is used to connect the post-catalyst UEGO sensor to the ETAS ES410 module. The four ETAS modules are daisy-chained together and connected to the INCA data acquisition system software with an Ethernet connection.

The sensors that came with the Honda engine are connected to the Woodward 128 pin ECU using the engine's original wiring harness. The engine controller code for the Woodward ECU is created with Matlab SIMULINK and the Motohawk development library. The Motohawk development library consists of proprietary blocks that allow SIMULINK to communicate with the Woodward ECU. The Mototune software is then used to flash the engine controller code onto the Woodward ECU. Mototune is also used to update calibration files for new engine controller code versions.

INCA is the user interface used for running the engine and recording data from the sensors connected to both the original wiring harness and the ETAS modules. INCA also allows users to control many of the parameters within the engine controller code, like the engine's air/fuel ratio and throttle position. INCA communicates with the Woodward ECU using the CAN Calibration Protocol (CCP). The computer loaded with the INCA software has a PCMCIA card that hardwires the computer to the CCP network.

The last data acquisition system is the Horiba MEXA 7500 emissions analyzer. The Horiba is able to measure total hydrocarbons, carbon monoxide in the low and high ranges, nitrogen oxides, carbon dioxide, oxygen and hydrogen. The Horiba is also equipped with two ovens, so two exhaust gas samples can be analyzed simultaneously. Therefore, emissions can be measured before and after the catalyst to determine the catalyst's conversion efficiency.

CHAPTER 4: MODEL OF THREE-WAY CATALYST OXYGEN STORAGE CHARACTERISTICS

The first step in creating a controller for the post-catalyst EGO sensor is to develop a model of the oxygen storage characteristics of the catalytic converter. A series of differential equations is used to create a catalyst model based on the conservation of mass. The model predicts the amount of oxygen stored inside the catalyst and the rate at which it is changing, using the mass airflow into the engine and reading from the pre-catalyst UEGO sensor. The oxygen storage model also provides an understanding of the plant necessary for control design and calibration. Once the oxygen storage model is completed, it can then be used to optimize the PI controller for the post-catalyst EGO sensor before the PI controller is placed in the engine controller code.

4.1 Model Structure

The overall structure of the model is shown in Figure 4.1. The first step in the model is to calculate the rate of net oxygen entering the catalyst. The rate of net oxygen is calculated with the following equation,

$$\dot{m}_{O2,in} = 0.23 \times MAF\left(1 - EQR_{in}\right) \qquad \text{Equation 4.1}$$

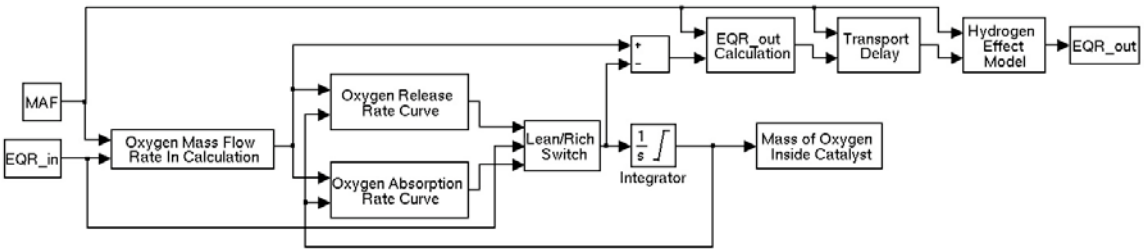

Figure 4.1: Structure of Catalyst Oxygen Storage Model

where $\dot{m}_{O2,in}$ is the rate at which net oxygen enters the catalyst, MAF is the mass airflow into the engine, and EQR_{in} is fuel/air equivalence ratio measured by the pre-catalyst UEGO sensor. If the engine is operating rich with an equivalence ratio greater than one, $\dot{m}_{O2,in}$ is a negative number and if the engine is operating lean with an equivalence ratio of less than one, $\dot{m}_{O2,in}$ is a positive number.

The second step in the model is to calculate the rate at which the catalyst releases and absorbs oxygen. The release and absorption rates are based on the current amount of oxygen stored inside the catalyst and the rate of new net oxygen entering the catalyst. If the engine is operating rich, with an equivalence ratio of greater than one, then the catalyst is releasing oxygen to bring the air/fuel ratio inside the catalyst back to stoichiometry. Equation 4.2 shows the catalyst releases oxygen at the maximum release rate if the absolute value of the rate of oxygen entering the catalyst, $\dot{m}_{O2,in}$, is greater than the maximum release rate, $\dot{m}_{\max,release}$. Otherwise, the catalyst releases enough oxygen to keep the air-fuel ratio inside the catalyst at stoichiometry until the catalyst is empty. The maximum oxygen release rate is experimentally determined and varies depending on how

much oxygen is stored inside the catalyst. The maximum release rate is the largest when the catalyst is full and zero when the catalyst is empty.

$$\text{if } \mathrm{EQR_{in}} > 1 \quad \dot{M}_{O2} = \begin{Bmatrix} -\dot{m}_{\max,release} & \left|\dot{m}_{O2,in}\right| > \dot{m}_{\max,release} \\ \dot{m}_{O2,in} & otherwise \end{Bmatrix} \qquad \text{Equation 4.2}$$

If the engine is operating lean, with an equivalence ratio of less than one, the catalyst is absorbing oxygen to bring the air/fuel ratio in the catalyst back to stoichiometry. Equation 4.3 shows the catalyst absorbs oxygen at the maximum absorption rate if the rate of oxygen entering the catalyst, $\dot{m}_{O2,in}$, is greater than the maximum absorption rate, $\dot{m}_{\max,absorb}$. Otherwise, the catalyst absorbs all net oxygen entering the catalyst until the catalyst is full. The maximum oxygen absorption rate is experimentally determined and varies depending on the amount of oxygen stored inside the catalyst. The maximum absorption rate is largest when the catalyst is empty and zero when the catalyst is full.

$$\text{if } \mathrm{EQR_{in}} < 1 \quad \dot{M}_{O2} = \begin{Bmatrix} \dot{m}_{\max,absorb} & \dot{m}_{O2,in} > \dot{m}_{\max,absorb} \\ \dot{m}_{O2,in} & otherwise \end{Bmatrix} \qquad \text{Equation 4.3}$$

Once the oxygen storage model has calculated the current oxygen release and absorption rates, the model looks at the equivalence ratio to determine if the engine is operating rich or lean. If the engine is operating rich, the model will use the oxygen release rate and if the engine is operating lean, the model will use the oxygen absorption rate.

The oxygen rate of change inside the catalyst is then integrated to determine the amount of oxygen stored inside the catalyst. The integration is shown in Equation 4.4, where M_{O2} is the amount of oxygen stored inside the catalyst.

$$M_{O2} = \int \dot{M}_{O2} dt \qquad \text{Equation 4.4}$$

The equivalence ratio of the exhaust gases exiting the catalyst is then calculated with Equation 4.5 and Equation 4.6. Equation 4.5 calculates the rate of net oxygen leaving the catalyst, $\dot{m}_{O2,out}$, by subtracting the rate of oxygen being absorbed or released, $\dot{M}_{O2}$, from the rate of oxygen entering the catalyst, $\dot{m}_{O2,in}$. Equation 4.6 calculates the equivalence ratio of the gases leaving the catalyst, EQR_{out}, using the mass airflow into the engine, *MAF*, and the amount of net oxygen leaving the catalyst, $\dot{m}_{O2,out}$.

$$\dot{m}_{O2,out} = \dot{m}_{O2,in} - \dot{M}_{O2} \qquad \text{Equation 4.5}$$

$$EQR_{out} = 1 - \frac{\dot{m}_{O2,out}}{0.23 \times MAF} \qquad \text{Equation 4.6}$$

The next step of the catalyst model is adding a transport delay to the EQR signal. The transport delay is the time it takes the exhaust gases to pass from the pre-catalyst UEGO sensor to the post-catalyst EGO sensor. The length of the transport delay depends on the speed of the air entering the engine. The faster the air enters the engine, the smaller the transport delay becomes.

The last step in the catalyst model is to simulate the filtering effects of the UEGO sensor. Unlike the simulated post-catalyst EQR signal, the EQR reading from the post-catalyst oxygen sensor does not instantaneously change from lean to stoichiometry or rich to stoichiometry. Therefore, a first order filter is applied to the simulated post-catalyst EQR signal to get the simulated signal to match up with the actual signal. Two different time constants are used with the first order filter. The first smaller time constant is used when the engine is switching from lean to rich and the second larger time constant is used when the engine is switching from rich to lean. The larger time constant is necessary when the engine is operating rich, due to the effect hydrogen has on the post-catalyst oxygen sensor. Both time constants vary with the mass airflow into the engine.

4.2 Data Processing

The catalyst's maximum oxygen storage capacity and oxygen release and absorption rates are experimentally determined using a set of pre and post-catalyst UEGO sensors. The sensors record the EQR of exhaust gases before and after the catalyst, as the engine's EQR is changed from lean-to-rich and rich-to-lean. The raw pre and post-catalyst EQR data sets are shown in Figure 4.2. Before the pre and post-catalyst EQR data can be analyzed, the data must first go through a series of data processing steps outlined in Figure 4.3.

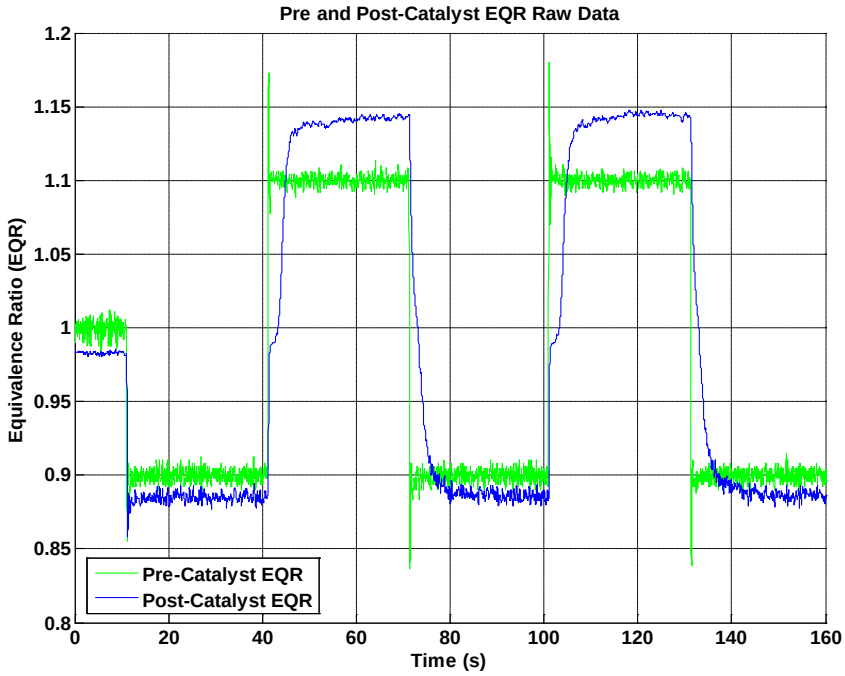

Figure 4.2: Raw Pre and Post-Catalyst Equivalence Ratio (EQR) Data

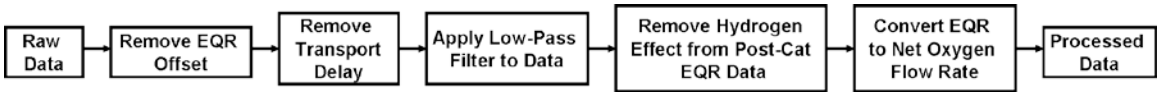

Figure 4.3: Flowchart of Data Processing Techniques

The first step in processing the raw EQR data is to make the stoichiometric point of the post-catalyst EQR data correspond to an EQR of one. The engine's stoichiometric point is when the EQR of the post-catalyst UEGO sensor plateaus after the EQR of the engine is changed from lean to rich, as shown in Figure 4.4. The plateau indicates the catalyst is releasing oxygen in order to keep the EQR of the gases inside the catalyst at stoichiometry. The EQR offset is partially caused by the hydrogen molecules in the exhaust gases interfering with the post-catalyst UEGO sensor reading (Buglass, Morgan and Graupner, 1998). Another cause for the EQR offset is the inaccuracy of the UEGO

sensor (Fiengo, Grizzle, Cook and Karnik, 2005). To remove this offset, 0.0105 is added to EQR of the post-catalyst data set.

The next step in processing the raw EQR data is removing the transport delay between the two sets of data, as shown in Figure 4.4. The transport delay is calculated by subtracting the time at which the pre-catalyst EQR data changes from lean to rich, from the time at which the post-catalyst EQR data changes from lean to rich. The post-catalyst

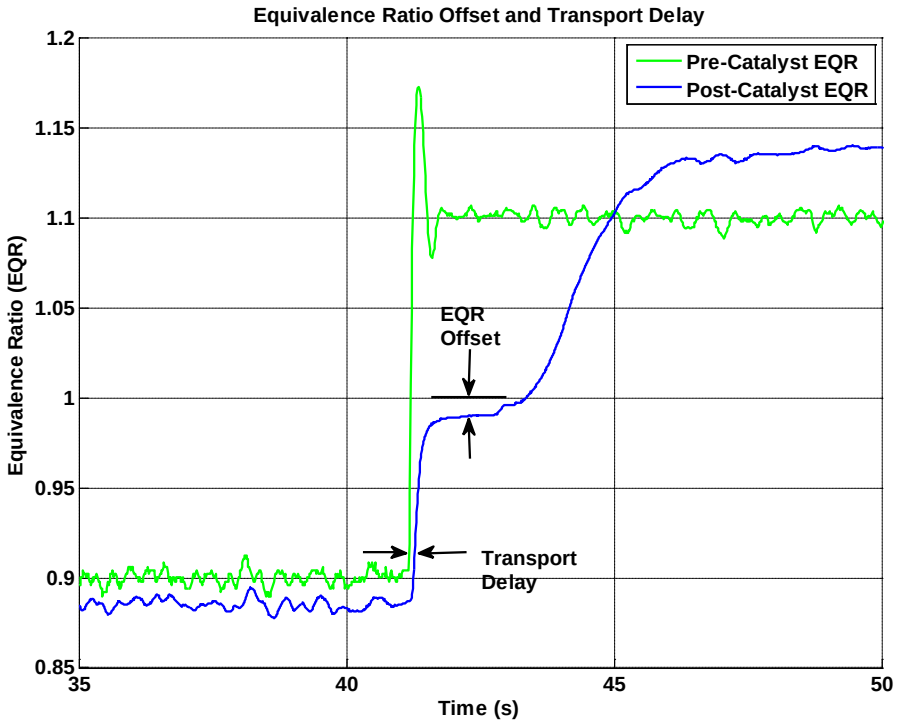

Figure 4.4: Equivalence Ratio Offset and Transport Delay between Pre and Post-Catalyst EQR Data

EQR data is then shifted backwards by the calculated time delay, so that the post-catalyst data lines up with the pre-catalyst EQR data.

Once the time delay is removed from the data, a fourth order low-pass butterworth filter is applied to both the pre and post-catalyst EQR data sets. The pre-catalyst EQR data is sampled at 72 Hz, and the filter for the pre-catalyst data has a normalized cutoff frequency of 0.25. The post-catalyst EQR data is sampled at 100 Hz, and the filter for the post-catalyst data has a normalized cutoff frequency of 0.40. The oxygen storage capacity of the catalyst filters the EQR of the exhaust gases before the EQR is measured by the post-catalyst oxygen sensor. Therefore, a lower cutoff frequency is applied to the pre-catalyst EQR data, because the pre-catalyst EQR data has more noise in it than the post-catalyst EQR data. Both normalized cutoff frequencies allow the noise in the two data sets to be filtered out, while the EQR changes due to actual engine events are preserved.

The next step in data processing is to remove the effect hydrogen has on the post-catalyst UEGO sensor data. When the engine has a rich EQR, the hydrogen generated inside the catalyst causes the post-catalyst UEGO sensor to measure an EQR greater than the actual EQR of the exhaust gases, as shown in Figure 4.5. Part of the hydrogen effect is removed from the post-catalyst data by multiplying the sections of the data with an EQR greater than one by a gain of 0.6 to 0.9. The gain allows the post-catalyst EQR data to have the same maximum value as the pre-catalyst EQR data when the engine is running rich. The hydrogen molecules also affect the measured post-catalyst EQR when the engine's EQR is changed from rich to lean. The post-catalyst UEGO sensor's rich to

lean EQR step should look similar to the post-catalyst UEGO sensor's lean to rich EQR step, instead of the gradual downward slope shown in Figure 4.5. To correct for the error, the post-catalyst EQR is set to one from when the post-catalyst EQR first starts to go lean to when the post-catalyst EQR is less than one, as shown in Figure 4.6.

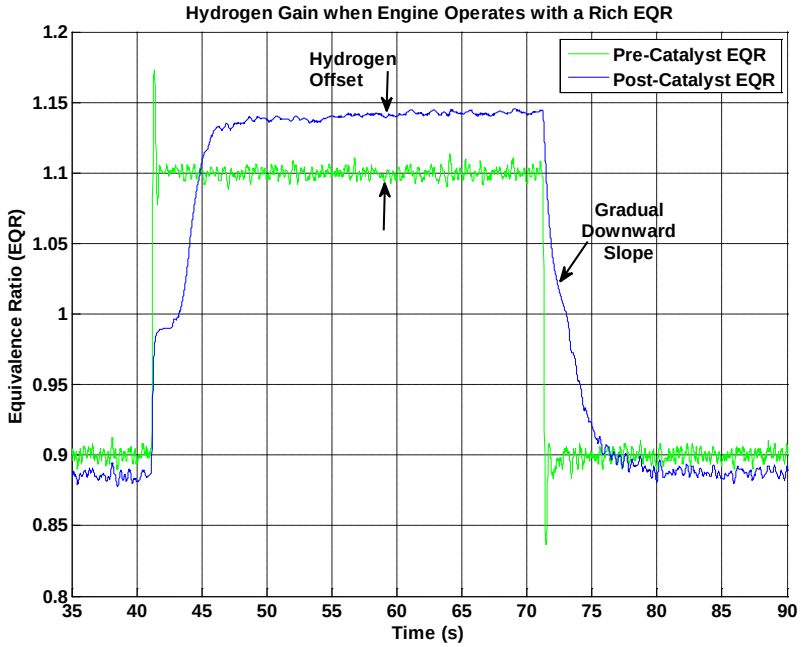

Figure 4.5: Effect of Hydrogen on the Post-Catalyst EQR Data when the Engine has a Rich EQR

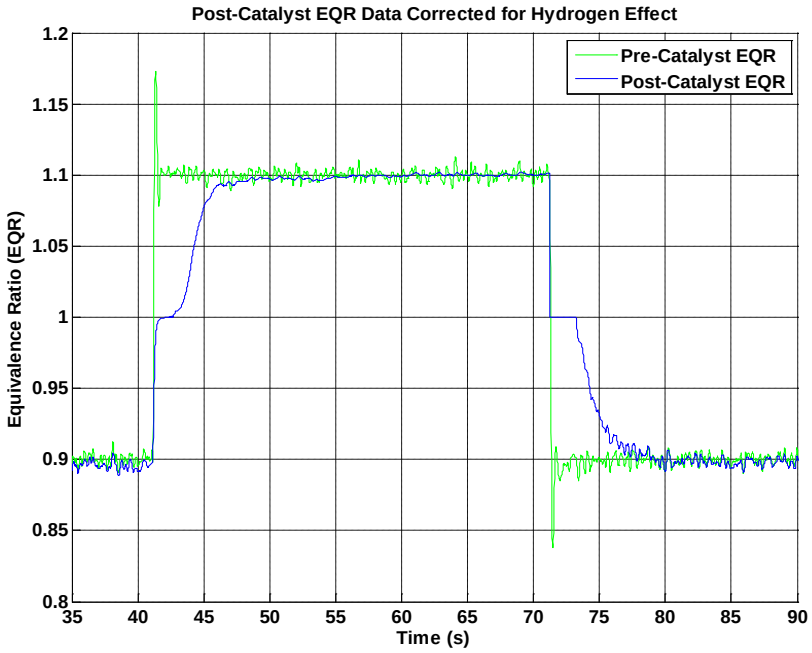

Figure 4.6: Post-Catalyst EQR Data Corrected for Hydrogen Effect

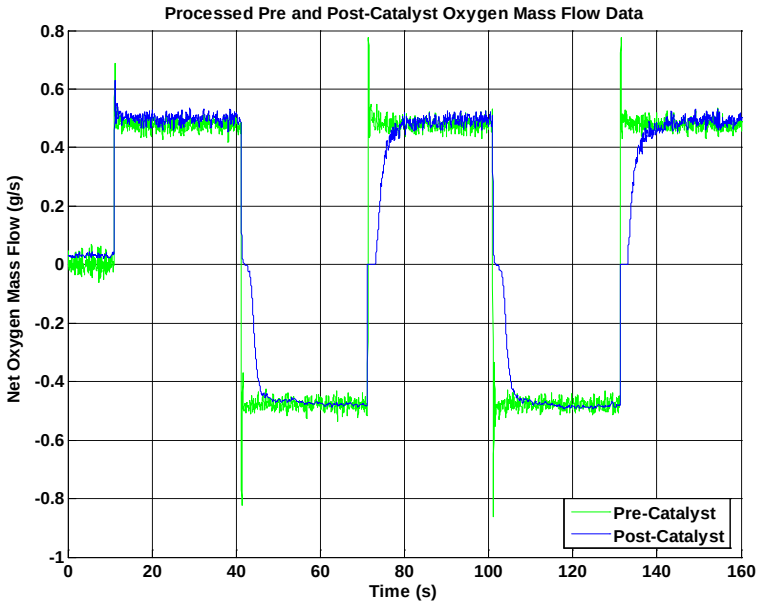

Figure 4.7: Processed Pre and Post-Catalyst Equivalence Ratio (EQR) Data

The final step in processing the pre and post-catalyst data is to convert the EQR data into an oxygen mass flow in grams per second. The engine mass airflow and measured EQR values are used with Equation 4.1 to do the conversion. The final processed data sets are shown in Figure 4.7.

4.3 Oxygen Storage Capacity

The maximum oxygen storage capacity of the catalyst is needed for the oxygen release and absorption rate curves, as well as the upper limit for the integration performed in the catalyst model. The maximum oxygen storage capacity of the catalyst is found by recording both the pre and post-catalyst UEGO sensor signals, while changing the engine's EQR from lean to rich and waiting for the catalyst to empty of all oxygen, as shown in Figure 4.7. Integration of the area between the pre and post-catalyst net oxygen flow rates gives the oxygen storage capacity of the catalyst for a specific set of engine operating conditions. A series of experiments were performed to determine the effect EQR step size, engine mass airflow (MAF), and exhaust gas temperature have on the maximum oxygen storage capacity of the catalyst.

The first series of oxygen storage capacity tests were to determine the effect EQR step size has on the oxygen storage capacity of the catalyst. Therefore, the mass airflow into the engine and the pre-catalyst exhaust gas temperature were held constant during the tests. The engine was operated at a speed of 1500 RPM and a load of 90kPa while the engine's EQR was changed from lean-to-rich in 2%, 4%, 6%, 8% and 10% EQR increments. For example, a 2% change in EQR indicates the EQR was changed from 0.98

to 1.02. The resulting oxygen storage capacities are shown in Figure 4.8. During each set of engine operating conditions, two lean-to-rich EQR steps and two rich-to-lean EQR steps were performed. The two lean-rich steps line up closely and have a gradual increase in O2 storage capacity from 1.85 to 2.31 grams as the EQR step size increases. However, the two rich-to-lean steps have a sharp increase in oxygen storage capacity from 1.56 to 2.78 grams as the EQR step size increases. Theoretically the lean-to-rich and rich-to-lean steps should have the same oxygen storage capacity, since the oxygen inside the catalyst cannot be created or destroyed. Therefore, the data processing techniques described in Section 3.2 were unable to eliminate all the effects the hydrogen molecules on the post-catalyst EQR data. Consequently, only the oxygen storage capacities from the lean-to-rich steps are used in the catalyst model.

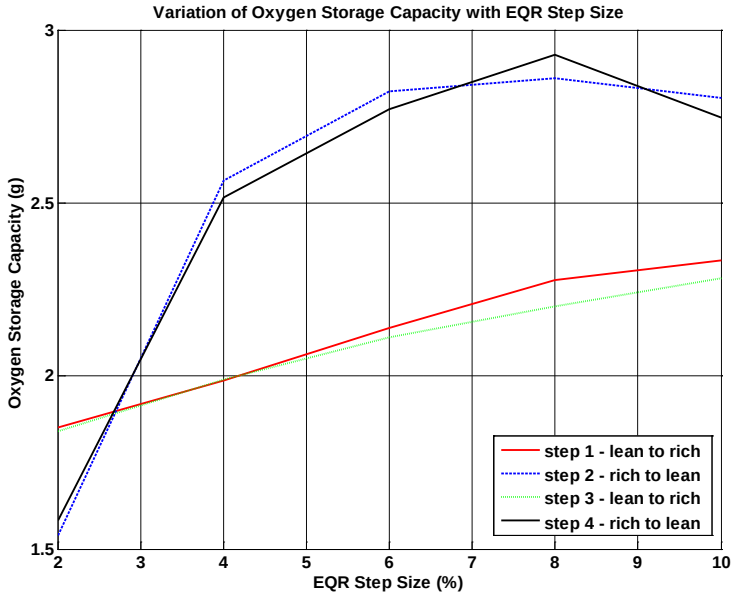

Figure 4.8: Variation in Oxygen Storage Capacity as a Function of EQR Step Size

The second set of tests was to determine the effect engine mass airflow had on the oxygen storage capacity of the catalyst. An EQR step size of 10% and an engine speed of 3000 RPM were used in each test, while the spark retard and engine load were varied to keep the pre-catalyst exhaust gas temperature as constant as possible. The results of the mass airflow tests are shown in Figure 4.9. At higher mass airflows, both lean-to-rich steps tend to have a constant oxygen storage capacity. However, at lower mass airflows the oxygen storage capacity first increases and then decreases with increases mass airflow. Also, there is always a 0.1 to 0.3 gram offset between the oxygen storage capacities of the two lean-to-rich steps.

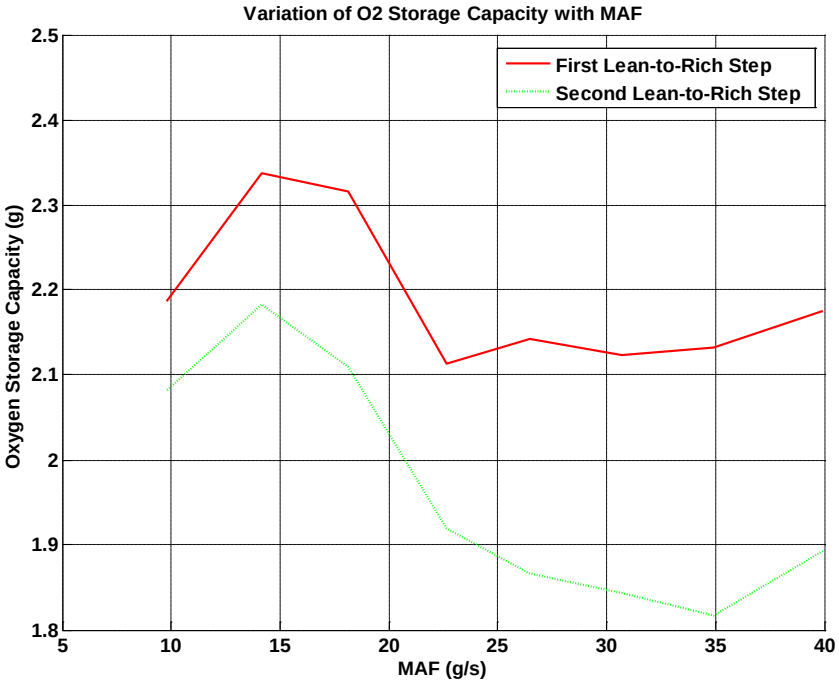

Figure 4.9: Variation in Oxygen Storage Capacity as a Function of Engine Mass Airflow (MAF)

The third set of tests was to determine the effect the pre-catalyst exhaust gas temperature has on the oxygen storage capacity of the catalyst. For each test, an engine speed of 1500 RPM, engine load of 90kPa and an EQR step size of 10% were used in order to keep the engine mass airflow constant. The spark retard of the engine was varied from 0 to 16 degrees to change the exhaust gas temperature during each test. The results of the exhaust gas temperature tests are shown in Figure 4.10. The results show there is no significant correlation between the pre-catalyst exhaust gas temperature and the oxygen storage capacity of the catalyst. The two lean-to-rich EQR steps also have an offset of 0.07 to 0.17 in their oxygen storage capacities.

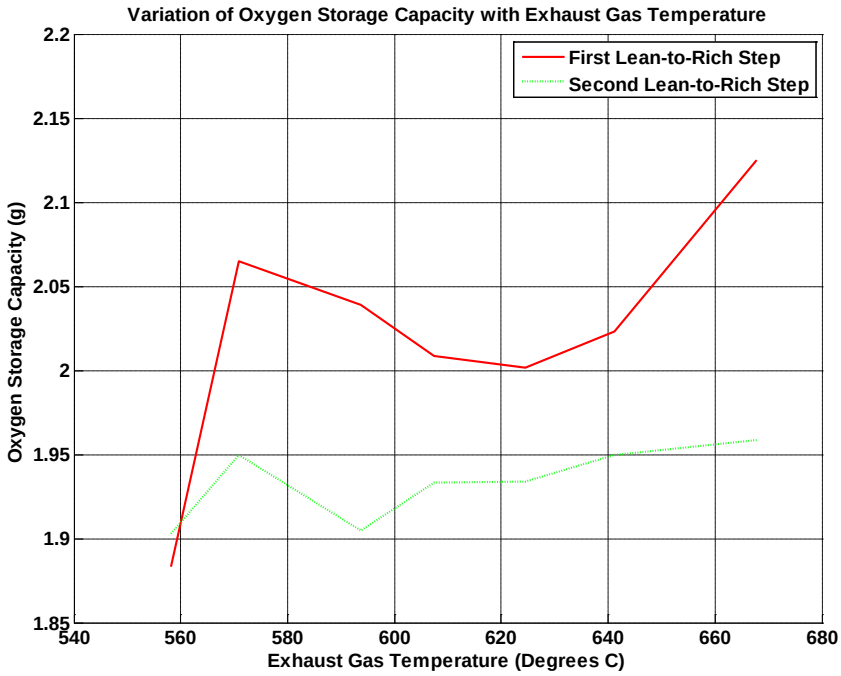

Figure 4.10: Variation in Oxygen Storage Capacity as a Function of Post-Catalyst Exhaust Gas Temperature

A fourth series of tests was done to determine why there was an offset in the oxygen storage capacities of the two lean-to-rich steps in the mass airflow and exhaust gas temperature experiments. In the fourth test, the engine was operated at 1500 RPM and a load of 90kPa. A series of four lean-to-rich EQR steps were completed, with an EQR step size of 10%. The engine was allowed to stay at each EQR level for one minute and thirty seconds, in order to ensure the catalyst reached steady state after each EQR command was given in the engine controller. The processed pre and post-catalyst EQR data is shown in Figure 4.11 and the calculated oxygen storage capacities are shown in Figure 4.12. The oxygen storage data shows something inside the catalyst is causing the catalyst's oxygen storage capacity to change between lean-to-rich steps, even though all engine-operating conditions were held constant. Hydrogen molecules interfering with the UEGO sensors could cause the difference in oxygen storage capacities between the different lean-to-rich steps. Additionally, any temperature variation within the catalyst substrate could also cause a difference in oxygen storage capacity. However, without more data no conclusions can be drawn.

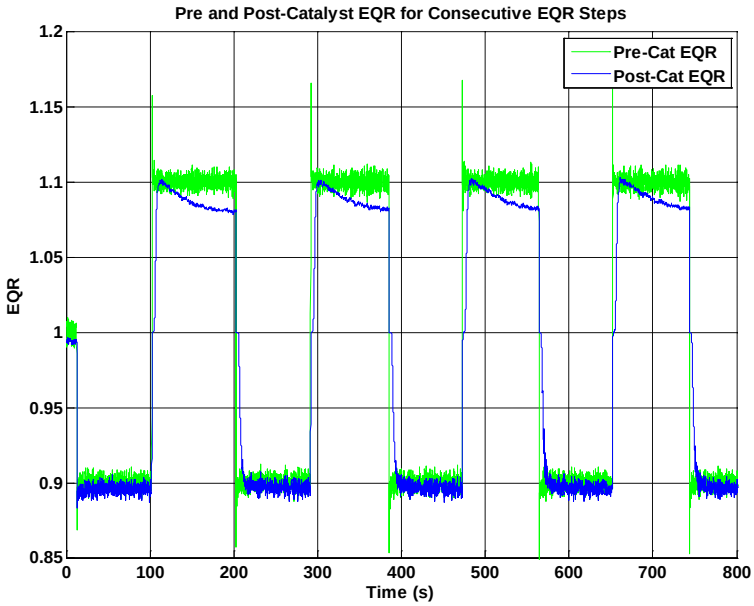

Figure 4.11: Processed EQR Data for Variation in Oxygen Storage Capacity caused by Hydrogen Molecules

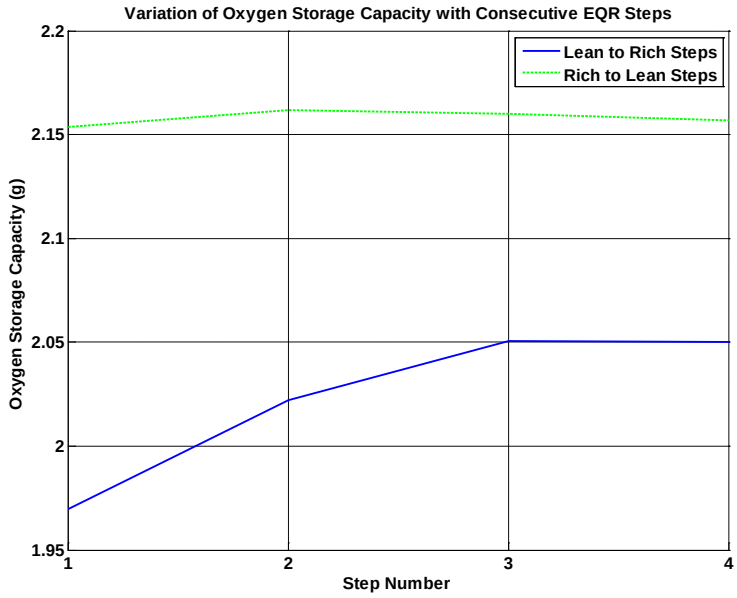

Figure 4.12: Variation in Oxygen Storage Capacity caused by Hydrogen Molecules

In the end, an average oxygen storage capacity of 1.93 was used in the catalyst model. An average capacity was used instead of a capacity that varied with exhaust gas temperature, mass airflow and EQR step size, due to the lack of defined trends in the oxygen storage data collected. The last oxygen storage test also showed that even when all variables in the engine controller are held constant, the oxygen storage calculations can still have a small amount of error in them.

4.4 Oxygen Release Rate Curve

The oxygen release rate curve determines how fast the catalyst model is able to release oxygen into the gases passing through the catalyst, when the engine's EQR is changed from lean to rich. The rate at which oxygen is released depends on the amount of oxygen currently stored inside the catalyst and the rate at which the EQR of the exhaust gases is changing. To accurately simulate the oxygen release behavior of the catalyst, a two-part release curve is used. The first part of the curve is a mass based curve shown in Figure 4.13 and the second is the normalized curve shown in Figure 4.14.

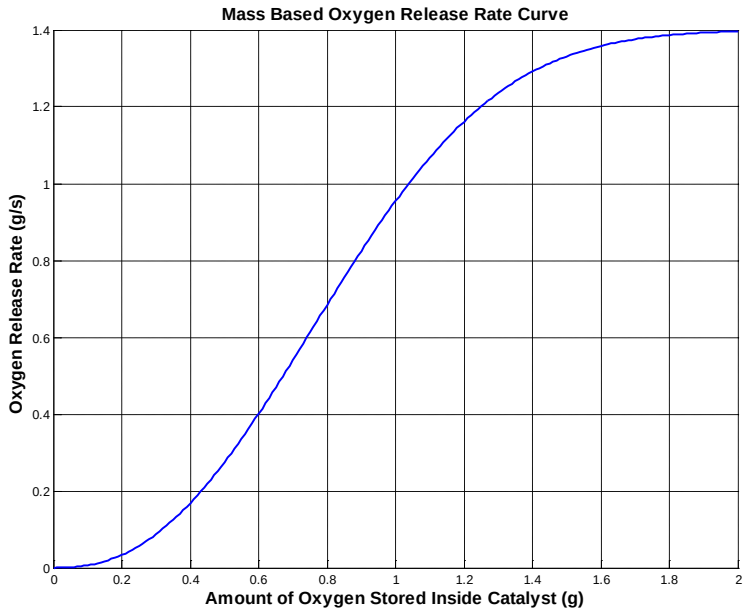

Figure 4.13: Mass Based Oxygen Release Rate Curve

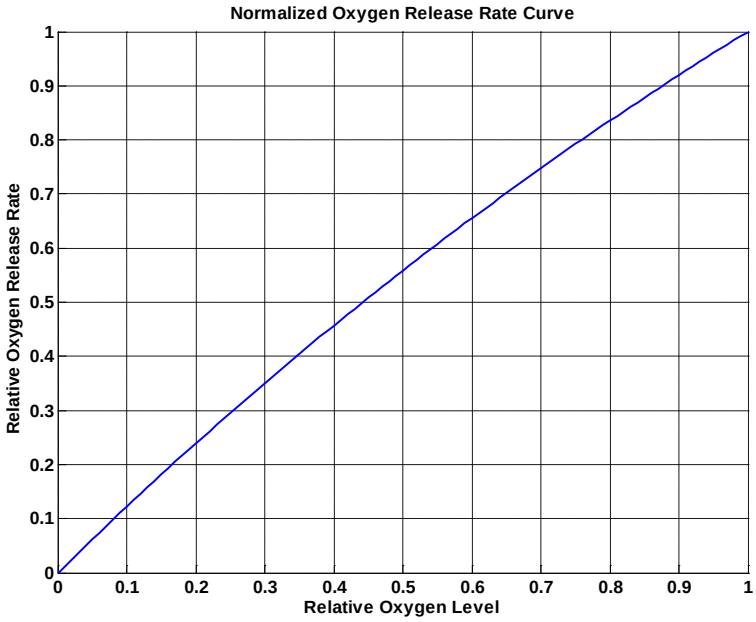

Figure 4.14: Normalized Oxygen Release Rate Curve

When the engine's EQR is changed from lean-to-rich, the model uses the mass based curve first. The model determines how much oxygen is currently stored in the catalyst and calculates the maximum oxygen release rate with the mass-based curve. If the rate at which oxygen is disappearing from the exhaust gases is less than the maximum oxygen release rate, then the model releases oxygen at the slower rate. The model continues releasing oxygen at the slower rate until the current oxygen release rate equals the maximum oxygen release rate, as shown in Figure 4.15. The model then takes the current oxygen storage level and release rate and multiplies them into the normalized release rate curve. The normalized curve then becomes massed based, as shown in Figure 4.15. The model continues to release oxygen at the rate indicated on the modified normalized curve until the catalyst is empty.

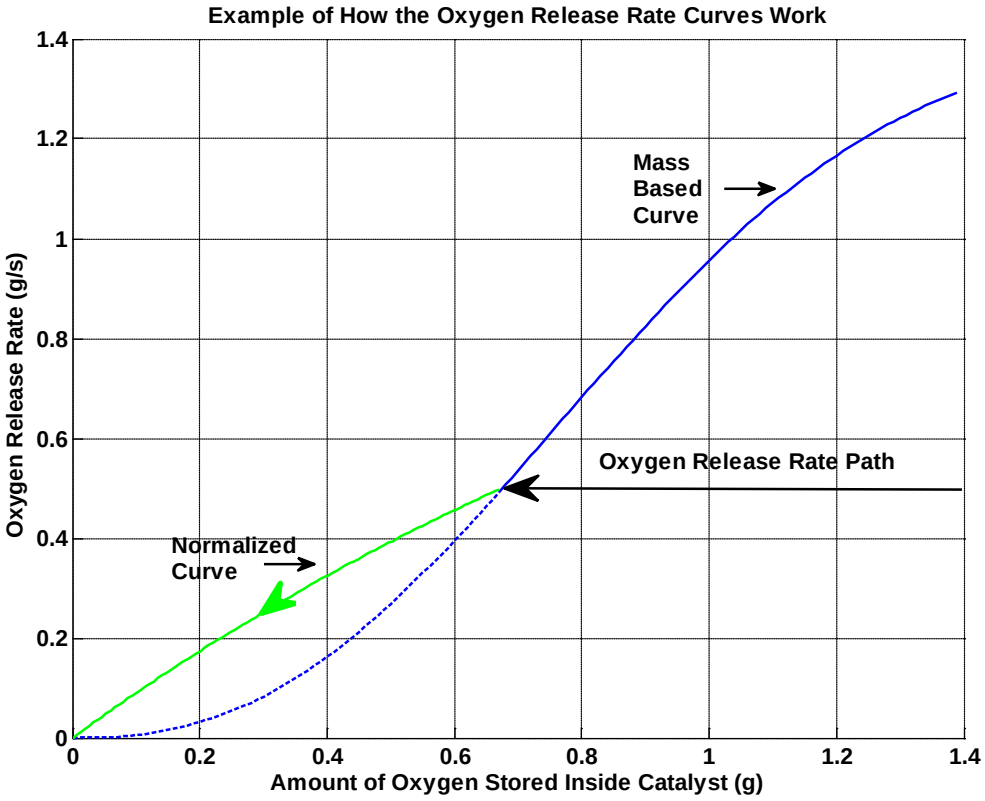

Figure 4.15: Diagram of How the Two Oxygen Release Rate Curves Work Together

4.4.1 Mass Based Oxygen Release Rate Curve

The mass based oxygen release rate curve was created by cumulatively integrating the area between the pre and post-catalyst oxygen mass flow rates shown in Figure 4.16. Like the oxygen storage calculations, only the lean-to-rich EQR steps were cumulatively integrated, because hydrogen molecules had made the rich-to-lean steps inaccurate. The resulting cumulative integration vector was then plotted against the change in the net oxygen mass flow rate between the pre and post-catalyst oxygen

sensors, as shown in Figure 4.17. The point at which the oxygen release rate leveled out to a constant value was then selected.

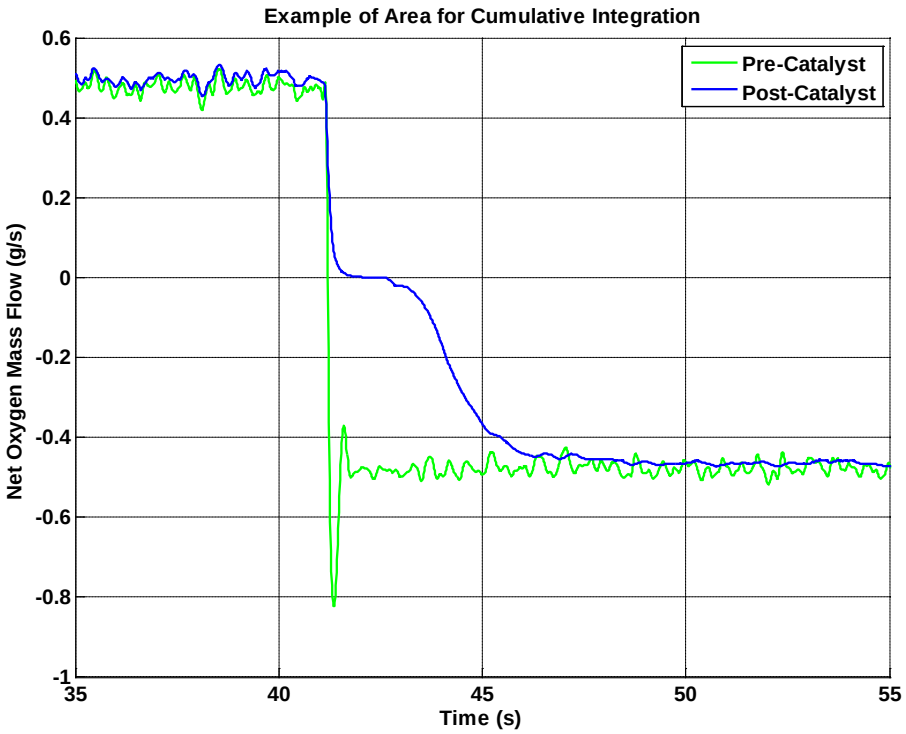

Figure 4.16: Example of Area for Cumulative Integration

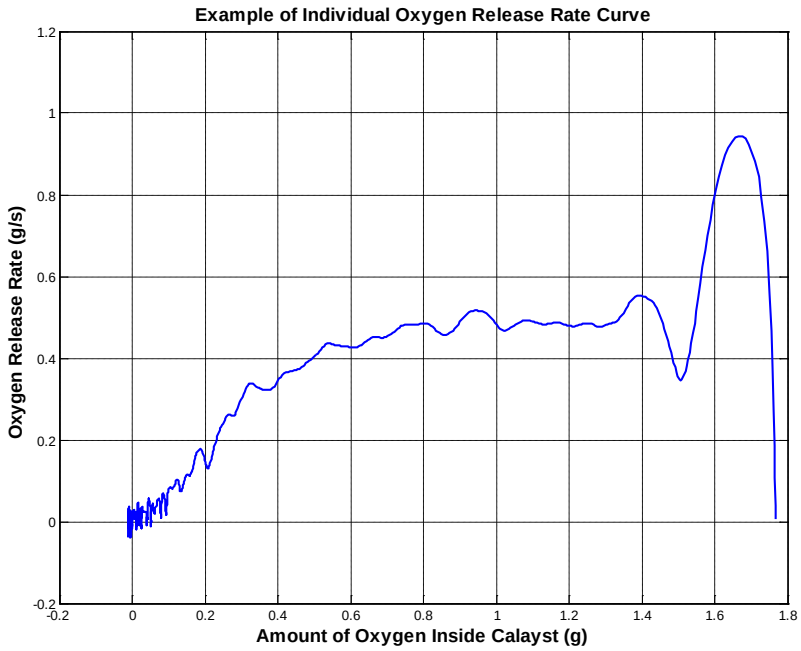

Figure 4.17: Oxygen Release Rate as a Function of Amount of Stored Oxygen

The cumulative integration process was performed on all the oxygen storage data collected, and the single points taken off of each graph were plotted in Figure 4.18. The Wiebe function was then fitted to the data points, creating the mass based oxygen release rate curve. The Wiebe function is shown in Equation 4.7, where $\dot{M}_{O2}$ is the oxygen release rate and M_{O2} is the amount of oxygen stored in the catalyst. The constants a, b and c in the Wiebe function are equal to 1.125, 0.991 and 2.435.

$$\dot{M}_{O2} = 1 - \exp\left[-a\left(\frac{M_{O2}}{b}\right)^{c}\right] \qquad \text{Equation 4.7}$$

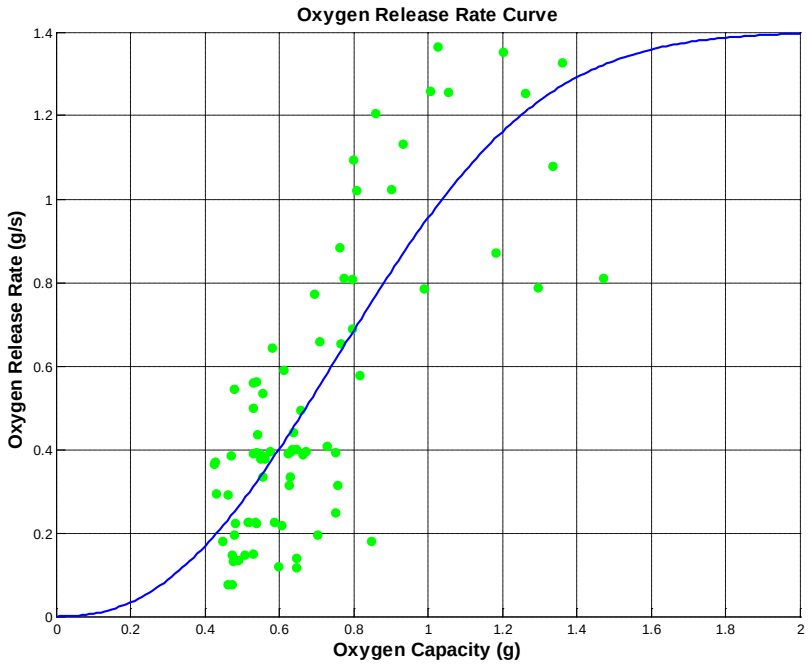

Figure 4.18: Mass-Based Oxygen Release Rate Curve with Data Points

4.4.2 Normalized Oxygen Release Rate Curve

To make the normalized oxygen release rate curve accurate in the engine's operating range, data was taken at 2000 RPM to get engine mass airflow rate in the 10 to 25 g/s range. The lean-to-rich EQR step data was then processed with the same cumulative integration technique used for the mass based oxygen release rate curve in Section 4.4.1. However, instead of selecting a single point off of the cumulative integration plot in Figure 4.17, all data points from when the catalyst is empty to when the oxygen release rate has zero slope were selected. The data points were then normalized, so each curve traveled from (0,0) to (1,1). The resulting curves are shown in Figure 4.19. Equation 4.8 was then used to create the normalized oxygen release curve. In

Equation 4.8, $\dot{M}_{O2,norm}$ is the normalized oxygen release rate, $M_{O2,norm}$ is the relative level of oxygen inside the catalyst and the constant ϑ is equal to 0.468.

$$\dot{M}_{O2,norm} = \frac{e^{-\vartheta \times M_{O2,norm}} - 1}{e^{-\vartheta} - 1} \qquad \text{Equation 4.8}$$

4.5 Oxygen Absorption Rate Curve

The oxygen absorption rate curve in Figure 4.20 is an inverted form of the mass based oxygen release rate curve shown in Figure 4.13. A new oxygen absorption rate curve was not created from experimental data. The hydrogen molecules generated inside the catalyst when the engine is operating with a rich EQR cause the EQR measured by

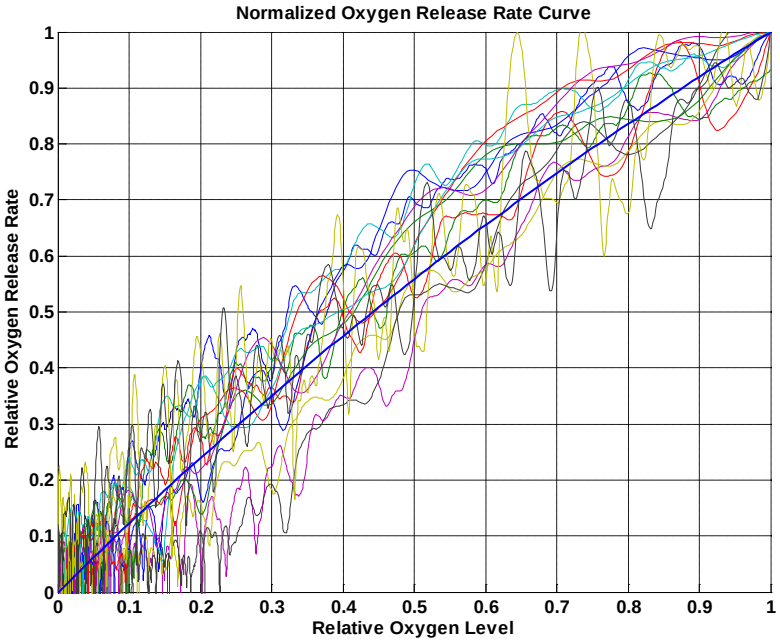

Figure 4.19: Normalized Oxygen Release Rate Curve with Data Points

the post-catalyst UEGO sensor to be inaccurate. Therefore, there is no way to know exactly what the measured post-catalyst EQR looks like when the engine EQR is switched from rich to lean.

The oxygen absorption rate curve functions the same way as the mass based oxygen release rate curve. When the exhaust gas's EQR is changed from rich to lean, the model determines how much oxygen is currently stored inside the catalyst and calculates the maximum oxygen absorption rate with the mass based curve. If the rate of net oxygen entering the model is less than the maximum oxygen absorption rate, then the model absorbs oxygen at the slower rate. The model continues to absorb oxygen at the rate it is entering, until the current oxygen absorption rate equals the maximum absorption rate. At that point, the model starts absorbing oxygen at the maximum rate indicated on the oxygen absorption curve until the model is empty.

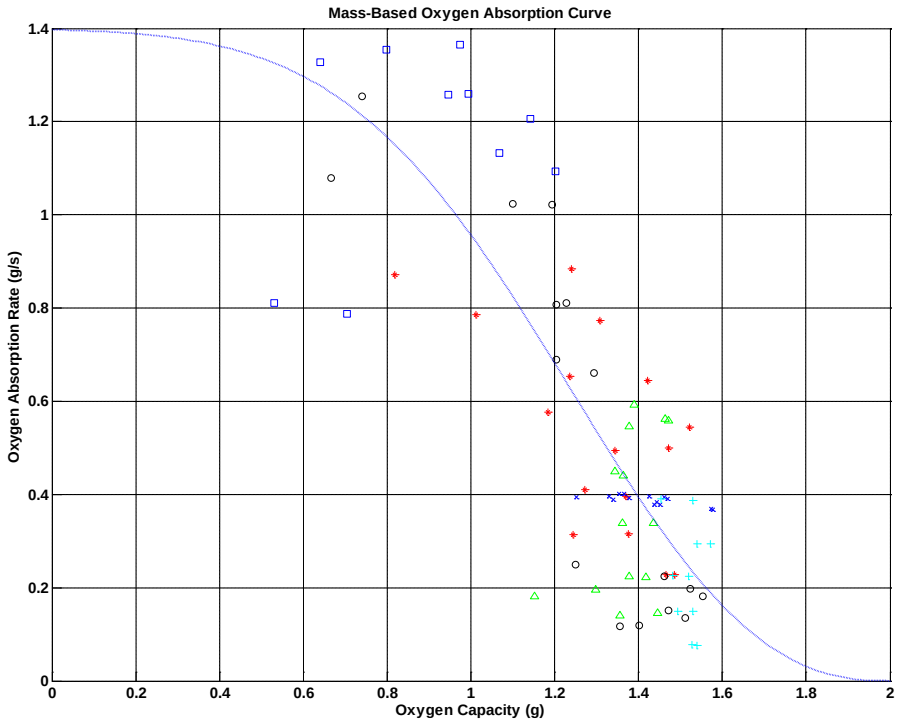

Figure 4.20: Mass Based Oxygen Absorption Rate Curve

4.6 Transport Delay

The transport delay between the pre and post-catalyst UEG sensors was calculated in the data processing described in Section 4.2. The transport delay for each data set was then plotted against its corresponding mass airflow into the engine, as shown in Figure 4.21. The faster air flowed into the engine, the shorter the transport delay between the two oxygen sensors. A fourth order polynomial was then fitted to the transport delay data, to account for the higher transport delays at low mass airflows. The fourth order polynomial is shown in Equation 4.9.

$$1.078\times10^{-7}x^4-1.804\times10^{-5}x^3+1.091\times10^{-3}x^2-2.855\times10^{-2}x+3.365\times10^{-1}=0 \quad \text{Equation 4.9}$$

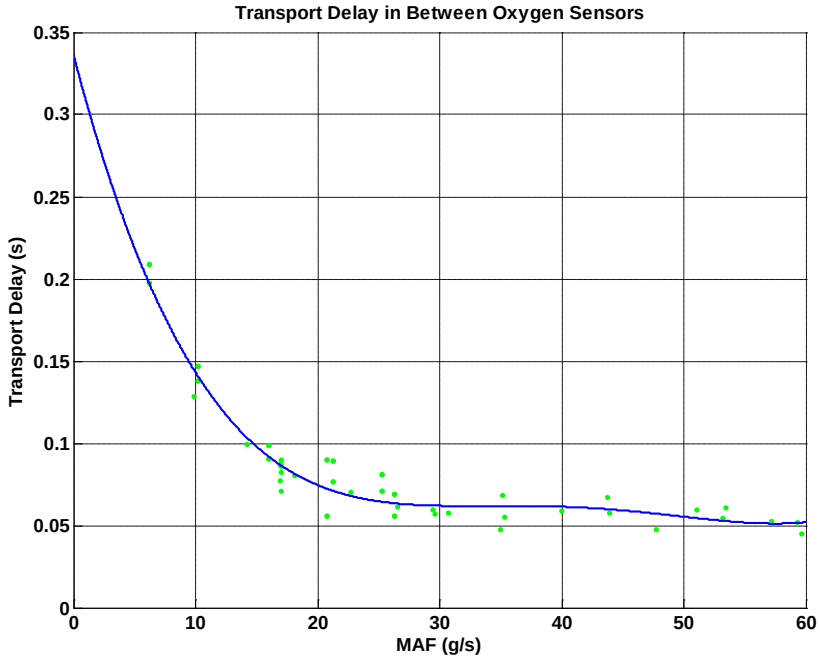

Figure 4.21: Variation in Transport Delay as a Function of Mass Airflow

4.7 Filtering the Simulated Post-Catalyst EQR

A first order filter is applied to the simulated post-catalyst EQR signal to simulate the response of oxygen sensors and the affect hydrogen molecules have on the oxygen sensor's response. The first time constant is used when the engine is operating lean. The first time constant is also used when the engine is operating rich and the catalyst is at steady state. The second time constant is used when the engine's EQR is changing from rich to lean. The second time constant allows the model to simulate the gradual EQR change seen by post-catalyst UEGO sensor, due to the hydrogen molecules interfering

with sensor's EQR measurement. Both time constants vary with the mass airflow into the engine.

The time constants were found by applying different time constants to the simulated post-catalyst EQR signal. The simulated signals were then visually compared to the actual post-catalyst EQR signal. The time constant that best captured the shape of the actual EQR signal was selected. The resulting time constants were then plotted against the MAF into the engine and a curve was fitted to the data. The time constants were found using the mass airflow experiment data taken when the engine was running at 3000 RPM.

The first time constant was found by comparing the simulated post-catalyst EQR signal to the actual EQR signal during the lean-to-rich EQR steps. A first order polynomial was then fitted to the data, as shown in Figure 4.22 and Equation 4.10.

$$-3.031\times10^{-3}x+1.809\times10^{-1}=0 \qquad \text{Equation 4.10}$$

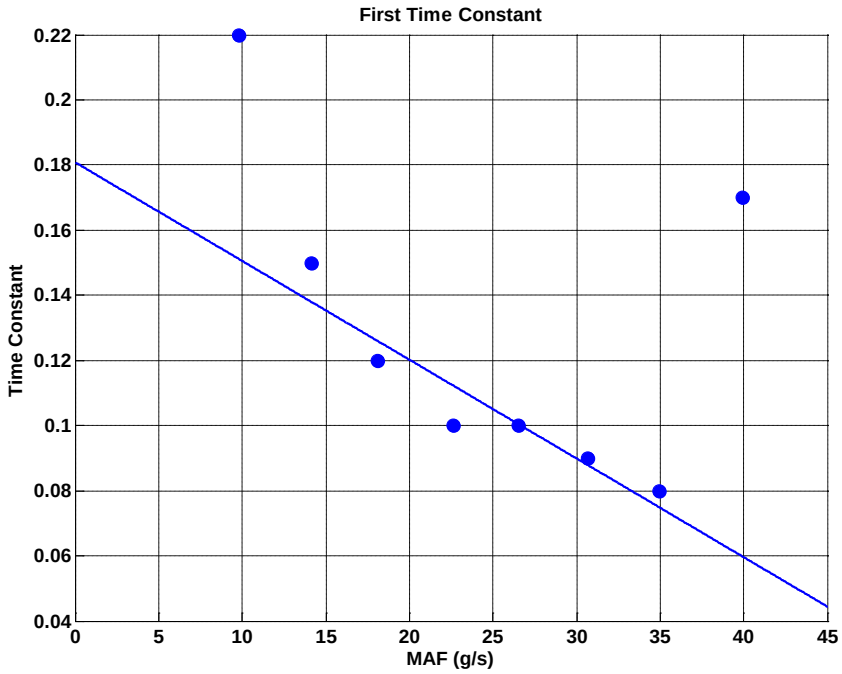

Figure 4.22: First Time Constant for Simulated Post-Catalyst EQR Filter

The second time constant was found by comparing the simulated post-catalyst EQR data to the actual signal during the rich-to-lean EQR steps. The resulting time constants and their corresponding mass airflows were then plotted in Figure 4.23 and the third order polynomial in Equation 4.11 was fitted to the data.

$$-1.261\times10^{-4}x^3+0.01164x^2-0.3793x+4.811=0 \qquad \text{Equation 4.11}$$

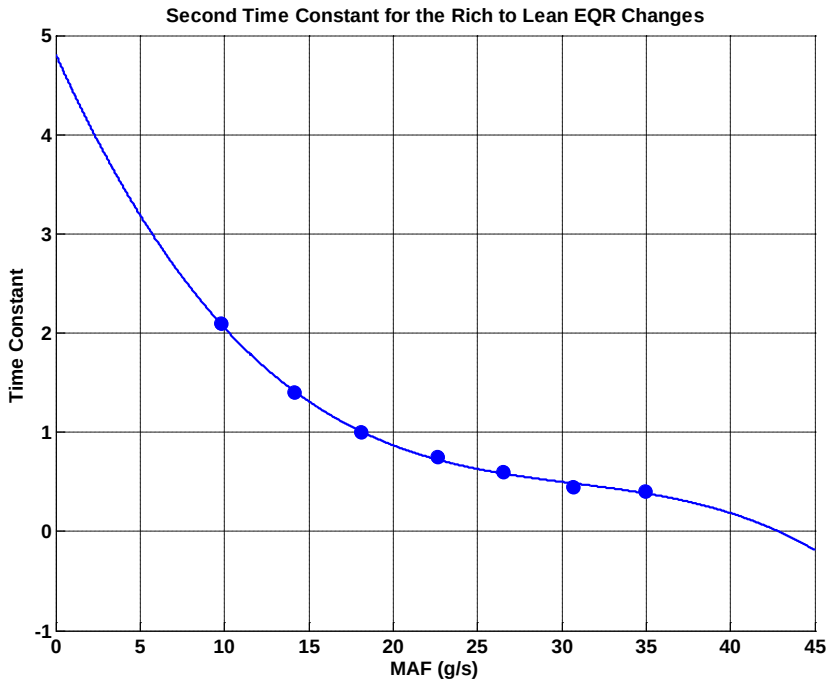

Figure 4.23: Second Time Constant for Simulated Post-Catalyst EQR Filter

4.8 Hydrogen Effects Acting on the Sensor

The hydrogen molecules generated inside the catalyst when the engine is operated rich cause the post-catalyst oxygen sensors to think the EQR of the exhaust gases is higher than it actually is. Therefore, the model must be able to simulate the effect hydrogen has on the post-catalyst oxygen sensor. To do this, a gain is applied to the post-catalyst EQR data when the gases exiting the catalyst have an EQR of greater than one. The data taken for the oxygen storage and oxygen release rate tests show the hydrogen gain can be between 1.087 to 1.695, depending on the EQR step size, mass airflow into the engine and the exhaust gas temperature. The data taken in the 2000 RPM range has an average hydrogen gain of 1.564. The engine will usually be operating around 2000 RPM

when it is in the EcoCAR vehicle, therefore the catalyst model uses the 1.564 hydrogen gain.

4.9 Validation of Catalyst Model

The catalyst model validation was done by comparing the data from the engine's post-catalyst UEGO sensor to the catalyst model's simulated post-catalyst UEGO sensor. The data used to validate the catalyst model was recorded when the engine was operating at 2000 RPM with a mass airflow rate between 11-25g/s. The 25 g/s case corresponds to the engine at wide-open throttle, while the 11 g/s case corresponds to an intake manifold pressure of 30-40 kPa. The validation data was taken at the 2000 RPM engine operating condition, because the engine will be operating around that engine speed inside the EcoCAR vehicle. Figure 4.24, Figure 4.25 and Figure 4.26 all show the results of the catalyst model validation. In each figure, the graph on the left shows the pre-catalyst UEGO sensor signal and the simulated post-catalyst UEGO sensor signal. The graph on the right compares the actual and simulated post-catalyst UEGO sensor signals.

Figure 4.24 shows the catalyst model can predict the post-catalyst UEGO sensor signal with a reasonable amount of accuracy when the engine has a mass airflow rate of 25 g/s and an EQR step size of 10%. The simulated and actual post-catalyst UEGO signals have slight differences during the lean-to-rich and rich-to-lean steps, but overall the simulated signal is able to capture the behavior the catalyst reasonably well. However, when the EQR step size or the mass airflow through the engine is decreased, the accuracy of the catalyst model decreases, as shown in Figure 4.25 and Figure 4.26.

The causes for the model's inaccuracy are the measured oxygen storage capacity of the catalyst, and the measured oxygen absorption and release rates.

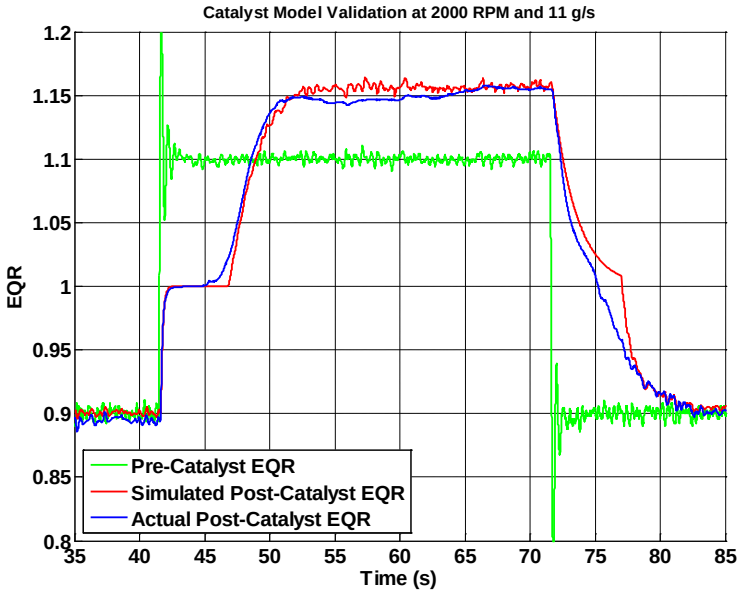

Figure 4.24: Catalyst Model Results for MAF of 25 g/s and EQR Step Size of 10%

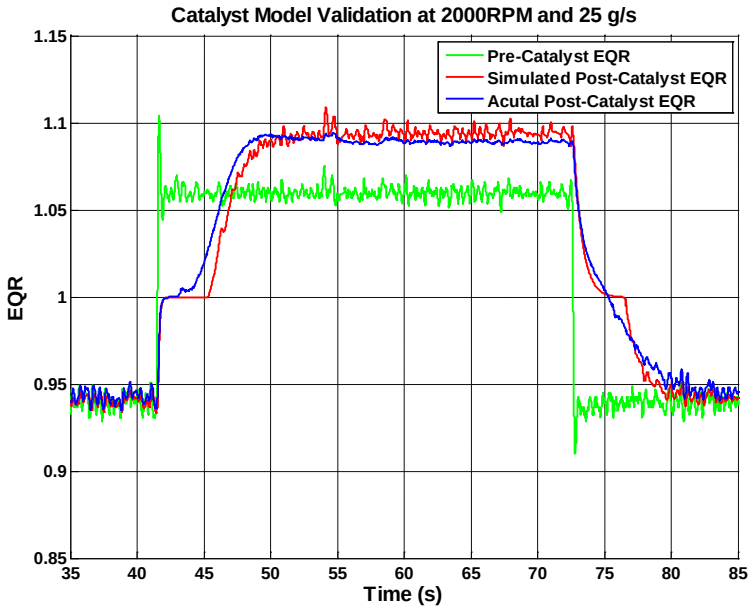

Figure 4.25: Catalyst Model Results for MAF of 25 g/s and EQR Step Size of 6%

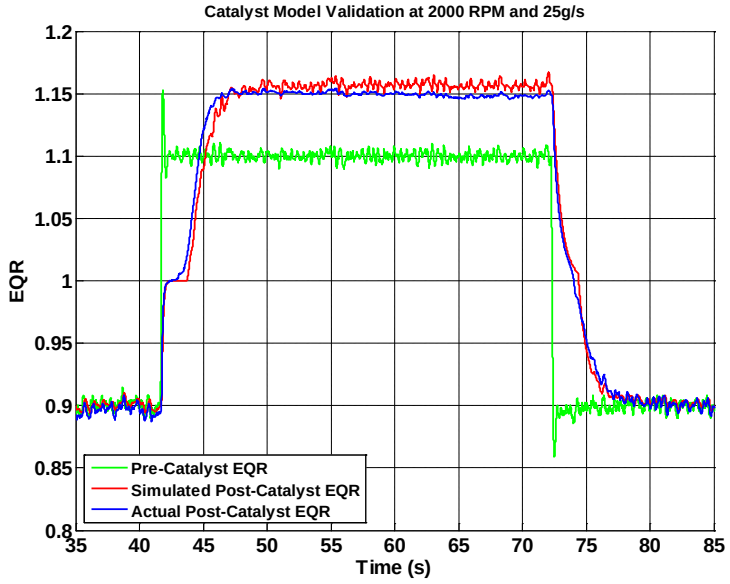

Figure 4.26: Catalyst Model Results for MAF of 11 g/s and EQR Step Size of 10%

Despite the inaccuracy of the catalyst model at different EQR step sizes and low mass airflow rates, the model is still able to capture the overall behavior of the catalyst in the 2000 RPM engine operating range. One important thing to keep in mind is the catalyst model is optimized to have the best accuracy within the 2000 RPM range, since the engine will be operating around 2000 RPM inside the EcoCAR vehicle. Although the model maybe able to predict the behavior of the catalyst outside of the 2000 RPM engine operating condition, the accuracy of the model will decrease.

CHAPTER 5: SOFTWARE VALIDATION OF THE CONTROL

The next step in creating a model of the post-catalyst EGO sensor controller is to create a simulation of it using the catalyst model created in Chapter 4. The post-catalyst EGO sensor controller is a PI controller that tracks an experimentally determined voltage set point. The structure of the simulated controller is similar to the structure of the controller in the actual engine code. Real EQR data taken from a vehicle is fed into the simulated controller, in order to simulate many of the transient EQR and mass airflow events that occur in an engine. An EQR disturbance is also applied to the EQR data to observe how the different proportional and integral controller gains cause the controller to react. The optimum proportional and integral controller gains are selected with the catalyst conversion efficiency curves for hydrocarbons, carbon monoxide and NO_x.

5.1 Post-Catalyst EGO Sensor PI Controller

5.1.1 Structure in Overall Engine Controller Code

Figure 5.1 contains a diagram of the overall engine control scheme. The controllers for the pre and post-catalyst oxygen sensors are both PI controllers. The feedback from both the pre and post-catalyst oxygen sensor controllers is used with a feed forward fuel controller to calculate the correct amount of fuel for each combustion

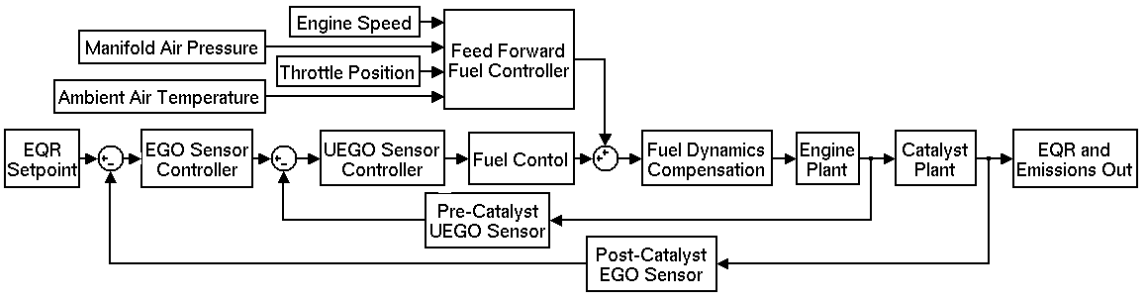

Figure 5.1: Structure of Overall Engine Controller Model

cycle. The feed forward fuel controller is used during transient conditions to predict how much air will be entering the cylinders at different engine operating conditions. The controller can then decide how much fuel should be added to the next combustion cycle using one of its predictions. The feed forward fuel controller is necessary because the overall engine controller needs to determine how much fuel to inject for the next combustion cycle before the engine gets to its new operating condition.

The first step in determining the amount of fuel for each cycle is to compare the voltage reading from post-catalyst EGO sensor to an experimentally determined EQR set point. The post-catalyst EGO controller then calculates the set point for the pre-catalyst UEGO sensor controller. The pre-catalyst UEGO sensor controller takes the EQR reading from the UEGO sensor and calculates a fuel multiplier that is sent to the fuel control of the engine. The fuel multiplier is used to make the amount of fuel injected into the next combustion cycle slightly rich or lean of stoichiometry, depending on the current air/fuel ratio of the engine. The command from the feed forward fuel controller is then added to the fuel control system to account for any transient conditions currently taking place in the engine. The resulting fuel command is then sent through a fuel dynamics

compensator. The fuel dynamics compensator is used to estimate how much of the injected fuel goes into the cylinders, and how much contributes to the fuel puddle in the intake manifold each combustion cycle. A modified fuel command comes out of the fuel dynamics compensator, and is set to the actuators for the fuel injectors. Fuel is then injected into the intake manifold port for the next combustion cycle and the resulting exhaust gases are expelled from the engine cylinders into the exhaust system. The exhaust gases pass through the catalytic converter and the two oxygen sensors, starting the air/fuel feedback loop over again.

5.1.2 Structure in Model

The structure of the simulated post-catalyst EGO sensor controller is shown in Figure 5.2. The main difference between the controller in the simulation and the overall engine code is the engine model in the simulation simplifies many of the processes happening in the engine. The engine model in the simulation combines the pre-catalyst UEGO sensor controller, the feed forward fuel controller and the fuel dynamics compensator from the overall engine code. To account for the dynamics in the engine model, real EQR and mass airflow data collected from a vehicle is used as the input to the engine model.

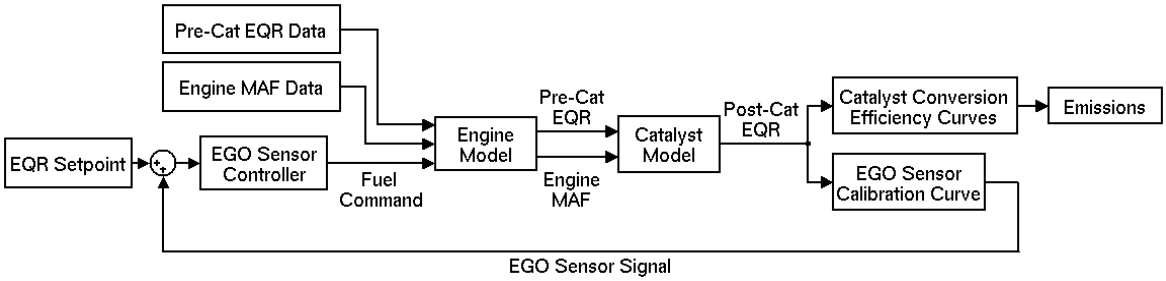

Figure 5.2: Structure of Post-Catalyst EGO Controller Simulation

The first step in the simulated controller model is to compare the predicted post-catalyst EGO sensor reading to the experimentally determined EQR set point. The EGO sensor controller then outputs a fuel command to the engine model block, which is shown in Figure 5.3. The engine control block takes pre-catalyst UEGO sensor data recorded from the engine and adds a disturbance to it. The fuel command is then multiplied into the resulting equivalence ratio to make the air/fuel ratio of the engine richer or leaner. The resulting product is the equivalence ratio read by the pre-catalyst UEGO sensor, which is then fed into the catalyst model. The engine block also reads mass airflow data recorded from the engine and feeds it into the catalyst model. The catalyst model then takes both the pre-catalyst EQR and engine mass airflow signals to calculate the EQR after the catalyst. The EGO sensor calibration curve is used to convert the EQR after the catalyst to the voltage reading of the EGO sensor. The EGO sensor signal is then fed back into the EGO sensor controller, completing the EGO sensor control loop. The amount of emissions given off by the vehicle is then estimated using the EQR after the catalyst and the catalyst conversion efficiency curves.

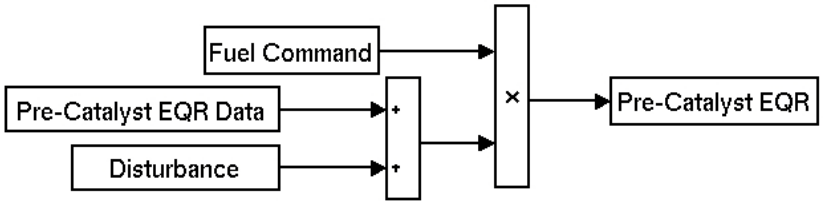

Figure 5.3: Structure of Engine Sub-Model

5.2 Calibration Curve for Post-Catalyst EGO Sensor

The calibration curve relating the exhaust gas EQR after the catalyst to the voltage output of the EGO sensor is shown in Figure 5.4. The calibration curve was found by recording the data from the post-catalyst UEGO and EGO sensors, as the engine's air/fuel ratio was changed from lean to rich multiple times. The UEGO and EGO data was then plotted against each other and the resulting UEGO-EGO curves were averaged together. The overall UEGO-EGO curve was then smoothed out to eliminate any spikes. The UEGO-EGO curve was also shifted to the left by 0.014, so that the initial EGO sensor set point of 694mV corresponded to an EQR of 1. The process for finding the EGO sensor set point is described in Section 5.3.

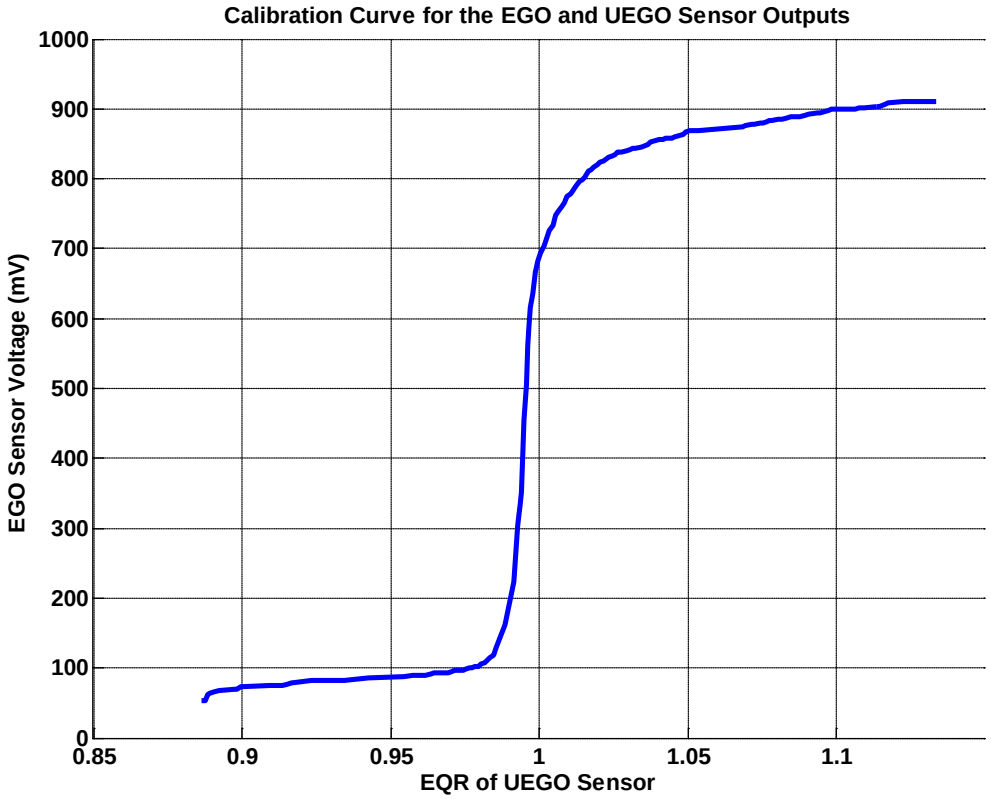

Figure 5.4: Calibration Curve EGO Sensor Output to EQR of Exhaust Gases After the Catalyst

5.3 Determination of Post-Catalyst EGO Sensor Set Point

The voltage set point for the EGO sensor was found by measuring the post-catalyst emissions as the EGO sensor controller tracked set points in ranging from 670-782 mV. The set point with the lowest overall emissions that could also be tracked by the EGO sensor controller over a range of operating conditions was then chosen. Figure 5.5 contains the average hydrocarbon, carbon monoxide and NO_x emissions at each set point. Both the hydrocarbon and carbon monoxide plots show that the amount of emissions increases as the voltage set point for the EGO sensor controller increases. The NO_x

emissions are all under 1.2 ppm. Although the catalyst-out emissions are the lowest in the 670 to 694 mV range, the EGO sensor controller is unable to track the lower set points without becoming unstable. Therefore, the initial set point for the EGO sensor controller is 694 mV. The set point for the controller may be raised to a higher voltage in the future, to make the EGO sensor controller more stable at specific operating conditions.

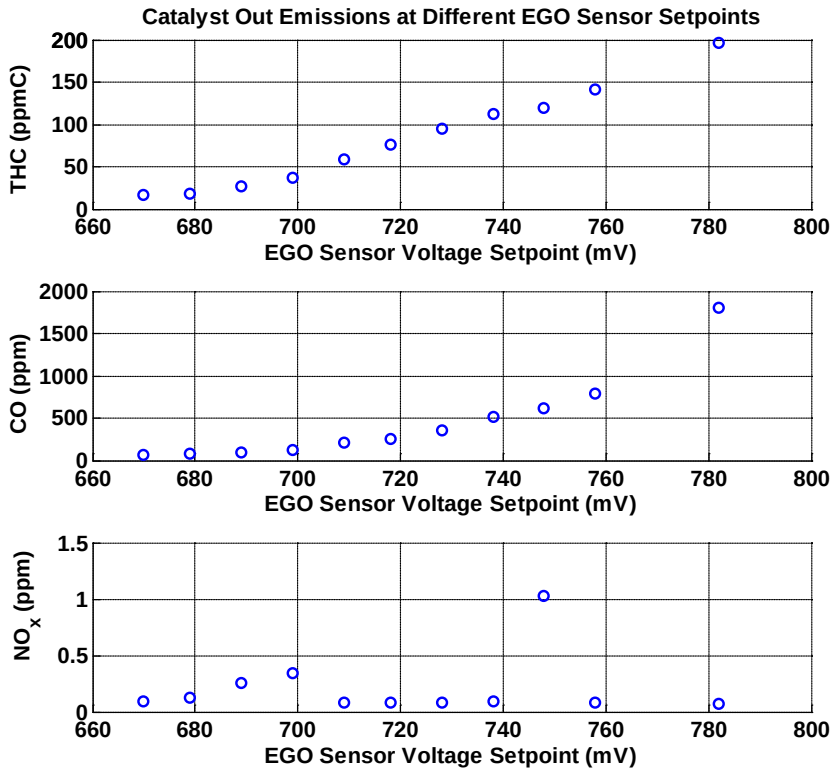

Figure 5.5: Catalyst-Out Emissions at Different EGO Sensor Set Points

5.4 Catalyst Efficiency Curves

The catalyst conversion efficiency used to estimate the amount of emissions exiting the catalyst are shown in Figure 5.6. The catalyst conversion efficiency curves are generic curves from the paper written by Erich Brandt, Yanying Wang and Jesse Grizzle. The unavailability of the emissions analyzer and the time constraints of this research project prevented the creation catalyst conversion efficiency curves specific to the catalyst used in this research.

The relative amounts of post-catalyst hydrocarbon, carbon monoxide and NOx emissions are estimated as shown in Figure 5.7. The current post-catalyst air/fuel ratio is used with the catalyst conversion efficiency curves in Figure 5.6 to find the current

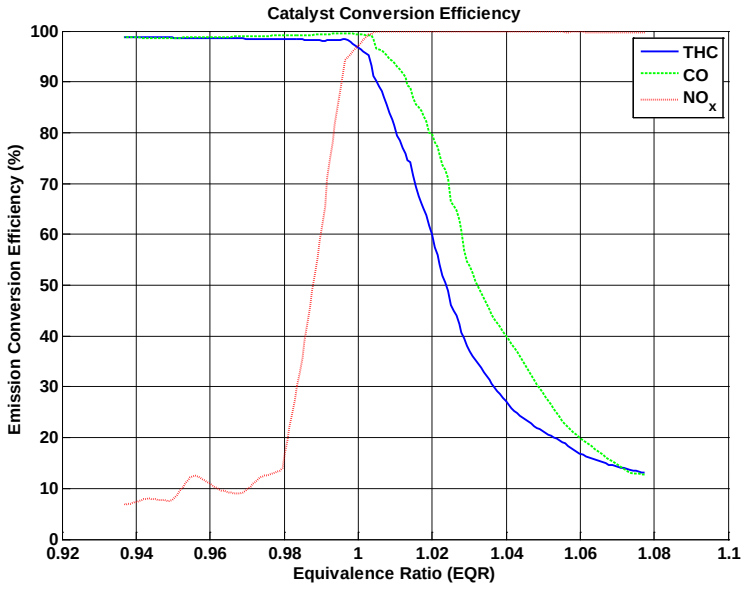

Figure 5.6: Catalyst Conversion Efficiency

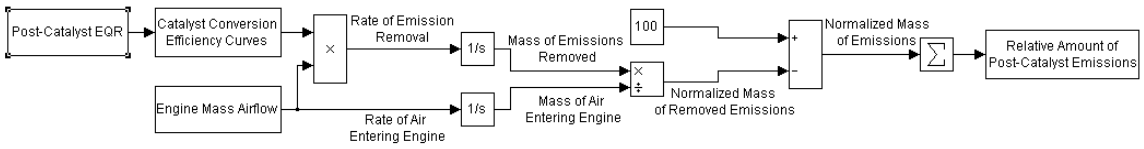

Figure 5.7: Calculation of Post-Catalyst Emissions Flowchart

catalyst conversion efficiencies for each pollutant. The catalyst conversion efficiencies for each of the three pollutants are then multiplied by the engine mass airflow to get the rate at which each emission species is removed from the exhaust gases. The rate of removal for each emission species is integrated, to get the mass of emissions removed by the catalyst from the exhaust gases. The mass of removed emissions is then divided by the mass of air entering the engine, to normalize data at different engine operating conditions. Therefore, each emission species can have a maximum removal of 100% from the exhaust gases leaving the catalyst. The percentage of emissions leaving the catalyst can be found by subtracting the removal percentage of each emission species from 100. The resulting percentages for each of the three emission species can be added together to get an estimate of the overall amount of emissions leaving the catalytic converter.

5.5 Results of Controller Model in Simulation

The simulation of the post-catalyst EGO sensor controller was used to gain a better understanding of how the controller's set point, proportional gain and integral gain influenced the output of the controller. Figure 5.8 contains the pre-catalyst EQR and engine mass airflow data used as inputs to the model. The data came from one of the

vehicles owned by the Center for Automotive Research, since data could not be collected from the EcoCAR vehicle due to mechanical problems with the vehicle's powertrain. The input data reflects multiple transient events that occurred in the vehicle, and thus represents the worst-case scenario for post-catalyst EGO sensor controller.

The effectiveness of the EGO sensor controller was determined by applying a +/- 2-4% EQR disturbance to the pre-catalyst EQR data over the course of the 1200-second simulation. The controller should be able to track the disturbance to bring the air/fuel ratio of the engine back to stoichiometry, if the controller has a good set point and

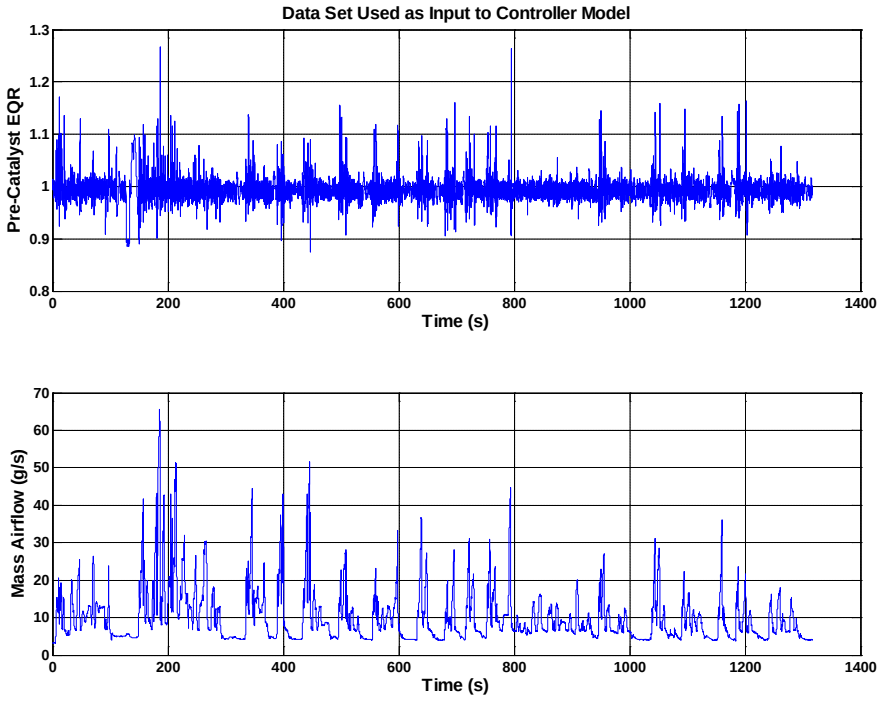

Figure 5.8: Worst Case Scenario Data Fed into Controller Model

proportional and integral gains. The main set point used in the simulation is the 694 mV set point found from the emissions testing in Section 5.3.

Figure 5.9 and Figure 5.10 contain the results of the simulation with a set point of 694 mV, a proportional gain of 0.0001 and an integral gain of 0.01. Figure 5.9 shows the set point and gains of the controller allow the controller to effectively correct for the increasing and decreasing EQR disturbance applied to the pre-catalyst EQR data. Figure 5.10 shows the output of the EGO sensor controller and the oxygen storage capacity of the catalyst work together to prevent lean and rich spikes in the post-catalyst exhaust gas EQR.

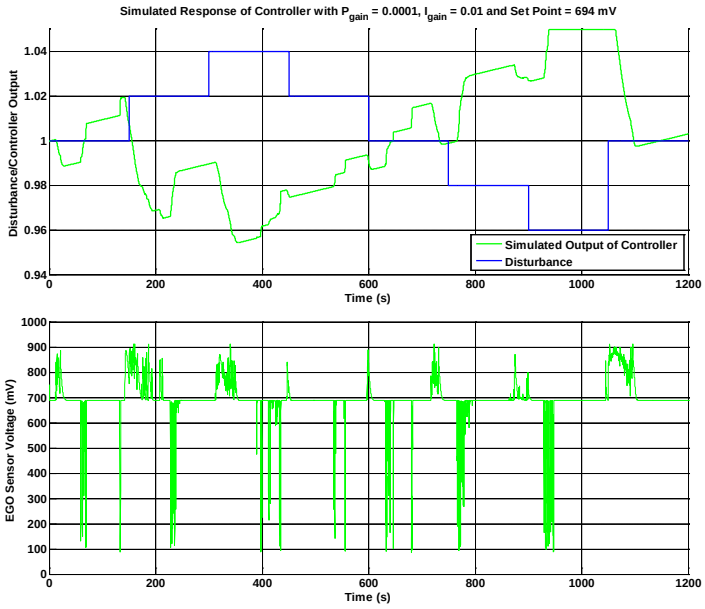

Figure 5.9: Simulated Response of the Controller Output for a P Gain of 0.0001, a I Gain of 0.01 and a Set Point of 694 mV

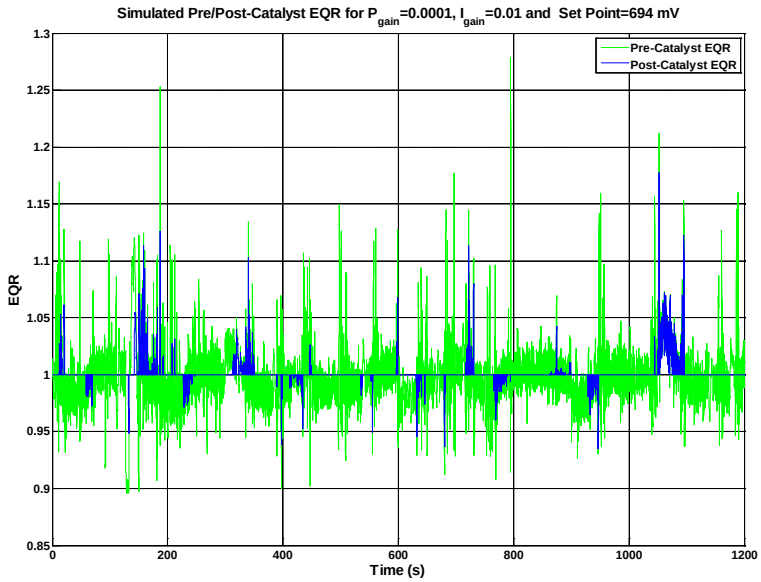

Figure 5.10: Simulated Pre and Post-Catalyst EQR Measurements for a P Gain of 0.0001, a I Gain of 0.01 and a Set Point of 694 mV

The EGO sensor controller simulation was run multiple times with a set point of 694 mV, and different combinations of the proportional and integral controller gains ranging from $10x10^{-3}$ to $10x10^{-6}$. At each combination of proportional and integral gains, the relative amount of emissions coming out of the catalyst was estimated using the procedure described in Section 5.4. The combination of gains with the lowest amount of emissions exiting the catalyst was considered to be the most effective at reducing emissions. The resulting data from the simulation was then combined into the contour plot shown in Figure 5.11. Figure 5.11 shows the integral controller gain has the most influence over the effectiveness of the EGO sensor controller at reducing emissions. Integral controller gains in the range of $10x10^{-3}$ to $10x10^{-4}$ were the most effective at reducing the emissions exiting the catalyst.

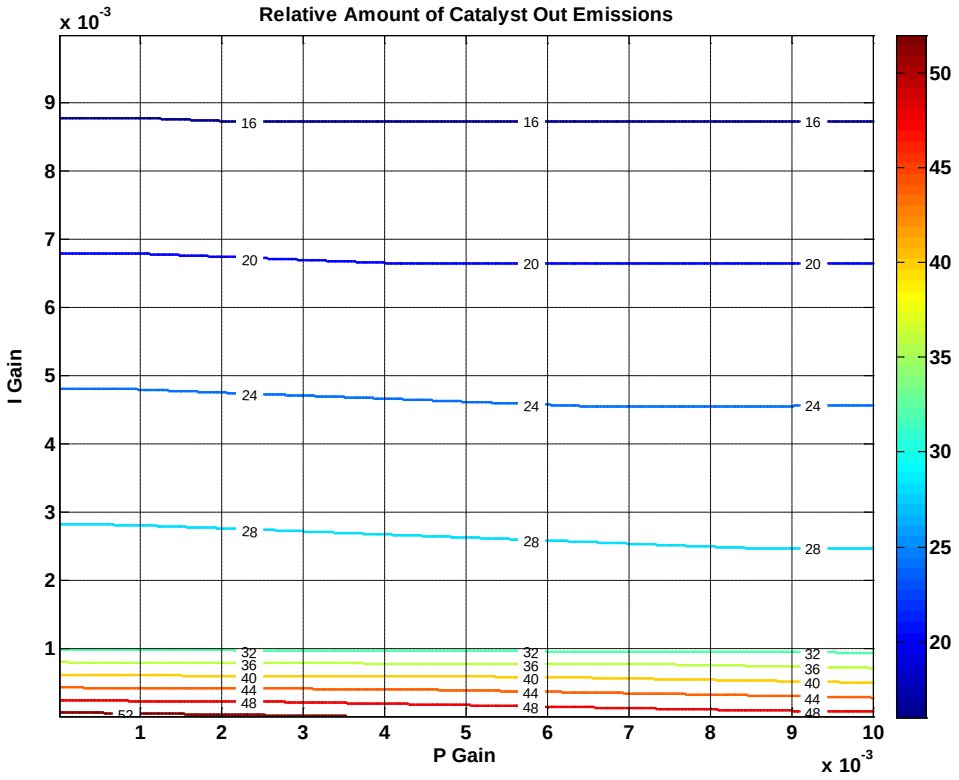

Figure 5.11: Relative Amount of Catalyst Out Emissions at Different Proportional and Integral Gains

However, when the optimum integral controller gains of $10x10^{-3}$ to $10x10^{-4}$ were used on the actual engine's EGO sensor controller, the output from the EGO sensor controller became unstable. The integral and proportional controller gains that made the engine's EGO sensor controller stable were 10 to 100 times smaller than the optimum gains from the simulation. The cause for the discrepancy between the simulated and actual EGO sensor controllers was not determined, thus the EGO sensor controller model was not validated. Despite the inaccuracies of the post-catalyst EGO sensor controller model, the model is still a useful in learning how the EGO sensor can be used to keep the

air/fuel ratio inside the catalyst at stoichiometry. The model can also be used to see how the oxygen storage capacity of the catalyst varies as different engine operating conditions and EQR disturbances are applied to the model.

CHAPTER 6: EMISSIONS TESTING

The emissions of the EcoCAR vehicle operating with the post-catalyst EGO sensor controller were estimated, to ensure the EcoCAR vehicle met the Environmental Protection Agency's (EPA) Tier 2, Bin 5 emission regulations. When this emissions testing was conducted the engine could not yet handle transient events, because the engine controller code did not contain transient air prediction software and fuel dynamics controllers. Therefore, it was assumed the vehicle was operating in series mode only for this emissions testing. The Horiba emissions analyzer was used to record post-catalyst emissions data over the 5-55 kW power output range of the engine. At each operating point, the EGO sensor controller tracked a voltage set point with different proportional and integral gains. The emissions data at each operating point was converted to an emissions rate in grams per second. The emission rates were then correlated to the power produced by the engine over the EPA's FTP-75 driving cycle, and integrated to get the total emissions produced by the vehicle during the drive cycle.

6.1 Emissions Testing Procedure and Data

The engine operating points used for emissions testing were selected from the series mode speed-torque curve shown in Figure 6.1. When the vehicle is operating in

series mode, the engine is connected to an electric motor and not directly connected to the wheels of the vehicle. Therefore, the engine is able to run at its most efficient operating points at all times. The engine's speed-torque curve was developed by combining the efficiencies of the engine and the electric motor the engine is connected to. The operating points at which the components had the highest combined efficiencies were then selected.

For emissions testing, operating points were chosen every 2-3 kW in the 5-55 kW power output range of the engine. The different combinations of EGO sensor controller set points, proportional, and integral gains used at the different operating points are listed in Table 6.1. The operating points with an engine power above 21 kW could all use the same set point, proportional gain and integral gain. However, the operating points at lower power outputs needed a higher voltage set point and slightly different proportional and integral controller gains, in order for the response of the EGO sensor controller to be stable.

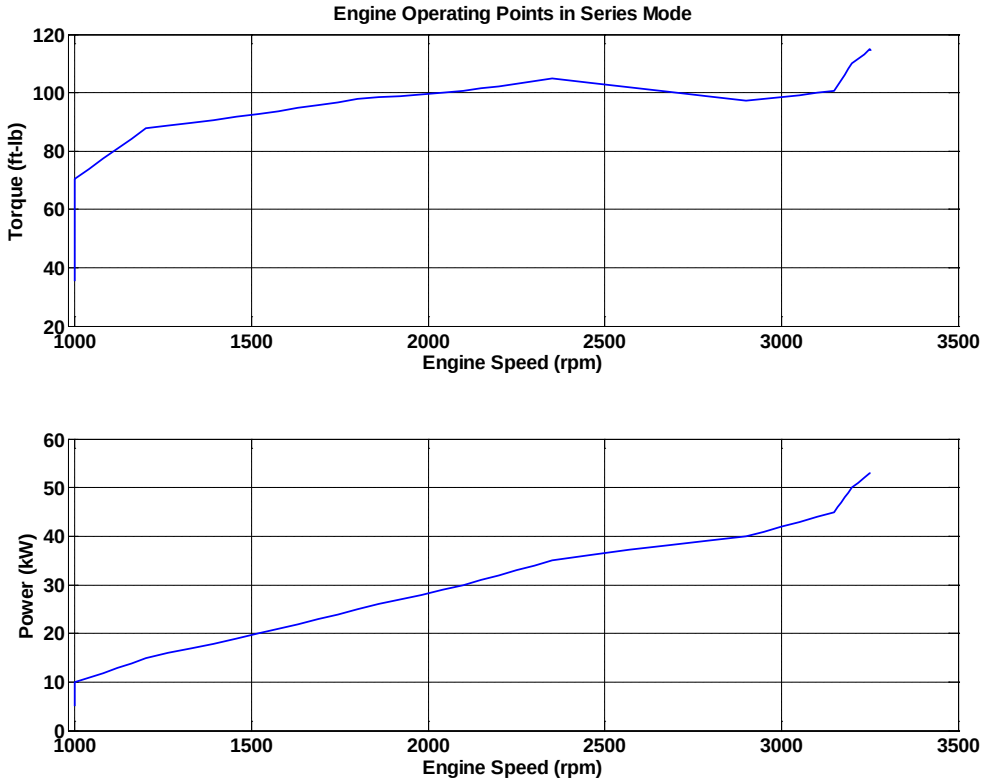

Figure 6.1: Engine Operating Points in Series Mode

Table 6.1: EGO Sensor Controller Set Points, Proportional and Integral Gains used during Emissions Testing

Engine Power (kW)	Set Point (mV)	Proportional Gain	Integral Gain
5-13	758	1.5E-05	1.0E-05
13	758	1.0E-05	1.5E-05
16-19	714	1.0E-05	1.0E-05
21-55	694	1.0E-05	1.0E-05

The Horiba emissions analyzer was used to record post-catalyst emissions data for thirty seconds at each operating point once the engine reached steady state. The average concentration of hydrocarbons, carbon monoxide and NO_x at each operating point was

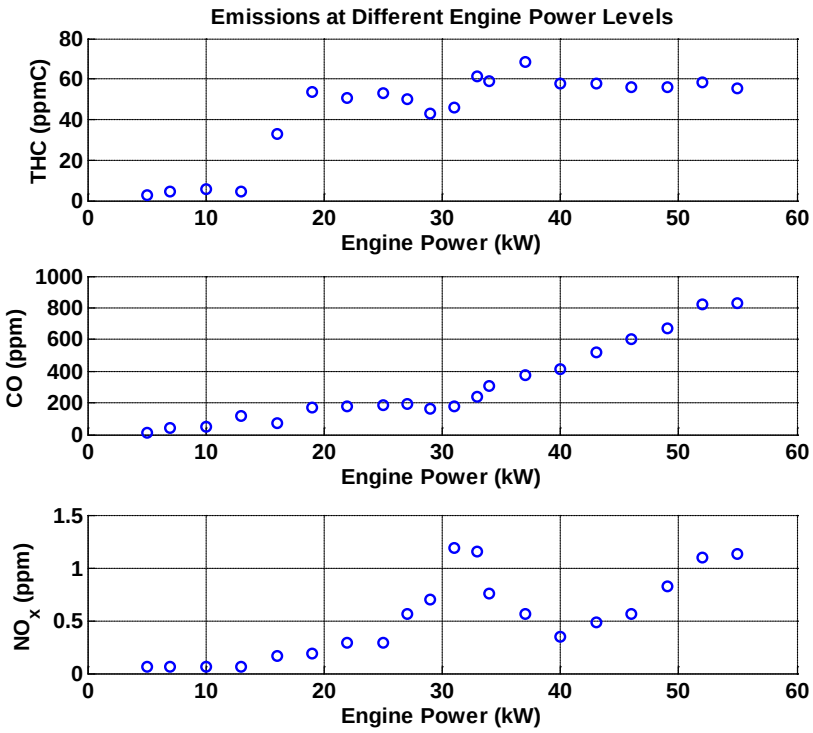

Figure 6.2: Emissions in Series Mode at Different Engine Power Levels

calculated, and the results were plotted in Figure 6.2. Figure 6.2 shows the concentration of hydrocarbons and carbon monoxide in the engine's exhaust gases increases, as the power output of the engine increases. The NO_x emissions do not exhibit a specific trend, but were always below 1.2 ppm at each engine operating condition.

The concentration of each emission species measured by the Horiba was converted into a mass flow rate using the following equation,

$$\text{Rate of Emission} = \frac{ppm_{emission}}{10x10^{6}} \times \left(1 + \frac{EQR_{post-catalyst}}{AFR_{stoich}}\right) \times MAF \times \frac{M_{emission}}{M_{exhaust}} \qquad \text{Equation 6.1}$$

where $ppm_{emission}$ is the concentration of the emission species, $EQR_{post\text{-}catalyst}$ is the equivalence ratio after the catalyst, AFR_{stoich} is the stoichiometric air/fuel ratio of E85, MAF is the engine mass air flow, $M_{emission}$ is the molar mass of the emission species and $M_{exhaust}$ is the molar mass of the exhaust gases. The resulting emission mass flow rates in grams per second at the different engine power outputs are shown in Figure 6.3. The rates of hydrocarbon, carbon monoxide and NO_x emissions all increase as the power output of the engine increases.

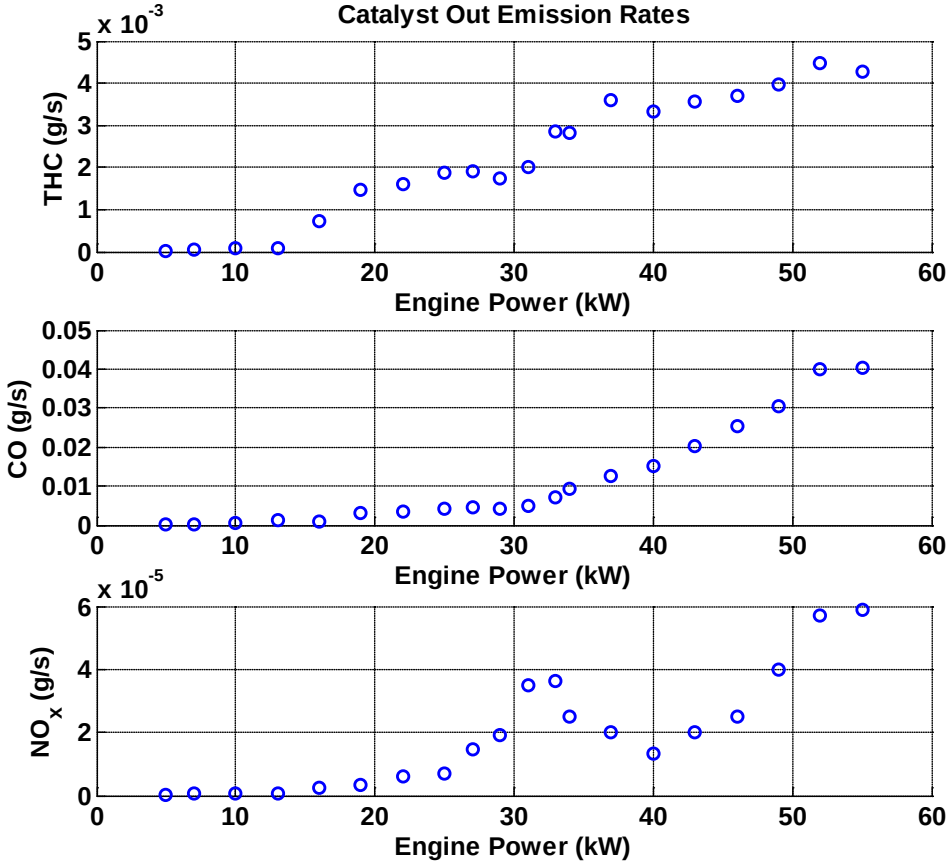

Figure 6.3: Rate of Emissions in Series Mode at Different Engine Power Levels

6.2 Estimate of the EcoCAR's Emissions in Series Mode

The EcoCAR competition guidelines require the EcoCAR vehicle to meet the EPA's Tier 2, Bin 5 emission regulations, which are listed in Table 6.2. The EPA requires vehicles in the Tier 2, Bin 5 category to have non-methane organic gas emissions (NMOG) less than 0.075 g/mile, carbon monoxide (CO) emissions less than 3.4 g/mile and NO_x emissions less than 0.05 g/mile. The total hydrocarbons measured by the Horiba emissions analyzer in the post-catalyst exhaust gases are directly compared with the EPA's NMOG emission standard in this analysis. However, the Horiba is only able to measure the total amount of hydrocarbons in the exhaust gases, which includes both methane and non-methane hydrocarbons. Therefore, the amount of NMOG emissions coming out of the catalyst is actually less than the total amount of hydrocarbons measured by the Horiba.

The Tier 2, Bin 5 emission regulations are measured over the FTP-75 drive cycle, which is shown in the first plot in Figure 6.4. The vehicle speeds required by the drive cycle were fed into the EcoCAR team's vehicle simulator to determine the speed and torque needed from the engine during the drive cycle, when the vehicle is operated in series mode. The torque and speed curves were then multiplied together to get the power needed from the engine during the FTP-75 drive cycle, which is shown in the second plot in Figure 6.4.

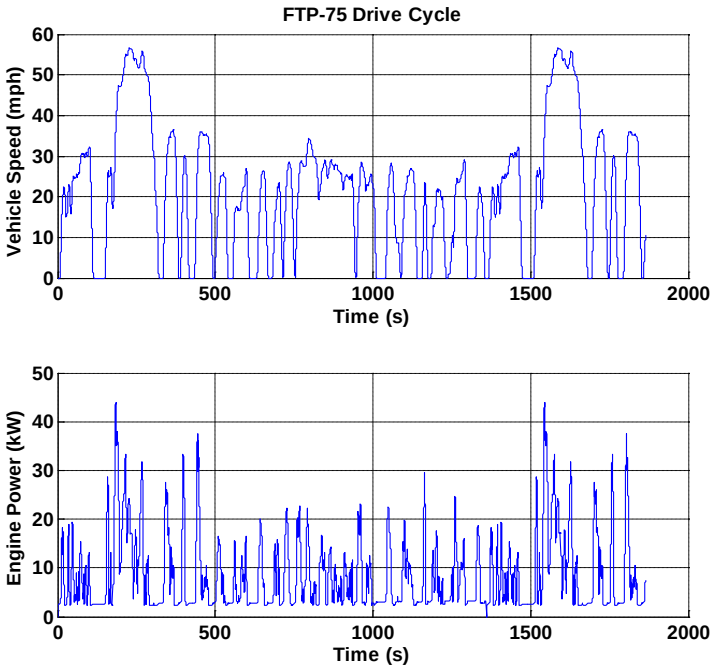

Figure 6.4: Speed and Power Traces for the EPA's FTP-75 Driving Cycle

The power requirements of the engine during the drive cycle were used with the rate of emissions exiting the catalyst in Figure 6.3 to determine the rate of catalyst out emissions over the FTP-75 drive cycle. Figure 6.5 shows the rate at which hydrocarbons, carbon monoxide and NO_x exit the catalyst during the FTP-75 drive cycle. The amount of emissions produced by the vehicle was calculated by integrating the rate of catalyst-out emissions over the drive cycle, and then dividing by the total distance traveled by the vehicle. The resulting emissions of the EcoCAR vehicle in series mode are listed in Table 6.2. The EcoCAR engine's hydrocarbon, carbon monoxide and NO_x emissions were lower than the limits set by the EPA. Therefore, the EcoCAR vehicle can meet the EPA's Tier 2, Bin 5 emission regulations when the vehicle is operating in series mode and the post-catalyst EGO sensor controller is enabled.

Table 6.2: Comparison of EcoCAR Vehicle Emissions to the EPA's Tier 2, Bin 5 Emission Regulations (U.S. Environmental Protection Agency, 2010)

	Non-Methane Organic Gas (NMOG) Emissions (g/mile)	**Carbon Monoxide (CO) Emissions (g/mile)**	**Oxides of Nitrogen (NO_x) (g/mile)**
EPA Tier 2, Bin 5	0.075	3.4	0.05
EcoCAR Vehicle	0.0546	0.1555	0.000363

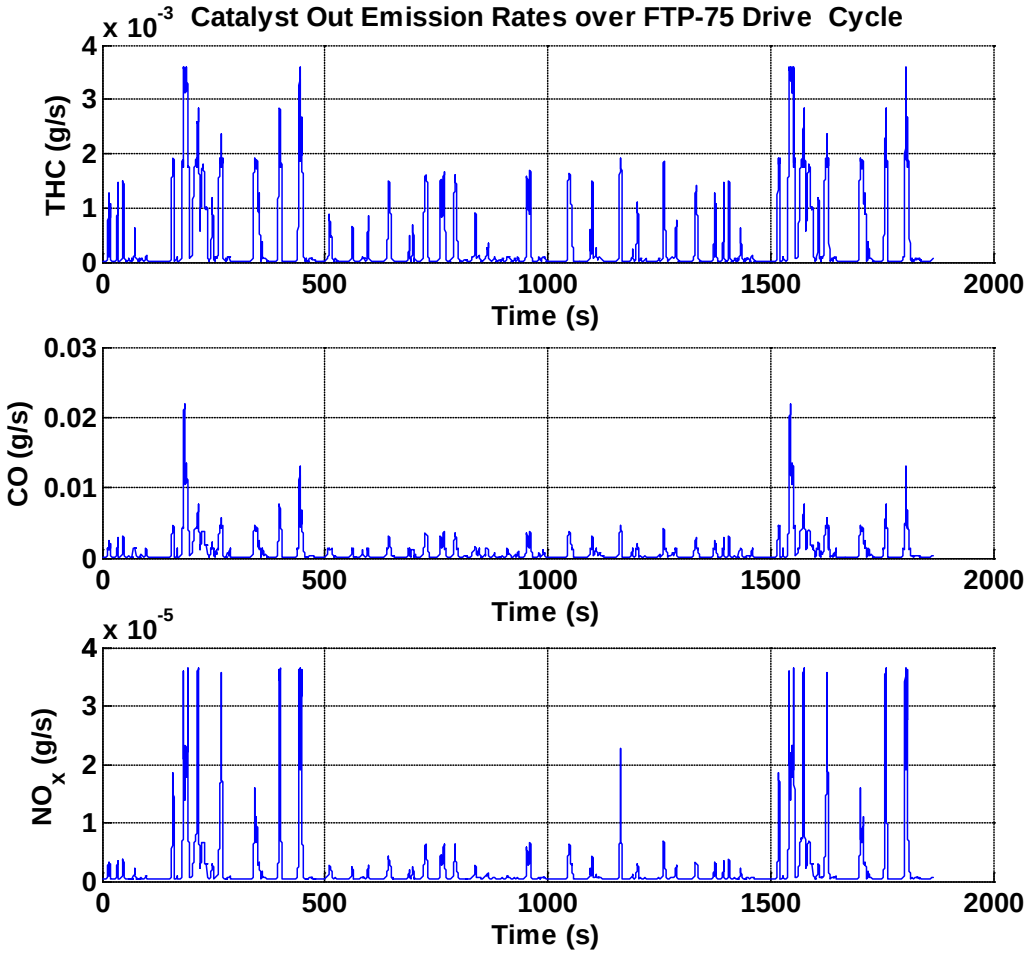

Figure 6.5: Series Mode Emissions during the EPA's FTP-75 Driving Cycle

6.3 Emissions Testing Summary

The results of the series mode emission tests showed the EcoCAR vehicle will be able to meet the EPA's Tier 2, Bin 5 emissions standards using the controller for the post-catalyst EGO sensor. The testing also showed that different combinations of the controller's set point, proportional and integral gain were needed to make the controller stable at different engine operating conditions. Therefore, the gains for the controller need to be scheduled with respect to different engine speed and load conditions, in order for the catalyst to a have high conversion efficiencies at all times.

CHAPTER 7: FUTURE WORK AND CONCLUSION

In conclusion, a PI controller for the post-catalyst EGO sensor was implemented in the engine controller code to reduce the emissions of the EcoCAR vehicle. The controller used the reading from the post-catalyst EGO sensor to determine if the engine was running either rich or lean of stoichiometry. The output from the EGO sensor controller was then used by the rest of the engine controller to adjust the amount of fuel injected into the engine during the next combustion cycle.

In order to create a simulation of the post-catalyst EGO sensor controller, a model of the oxygen storage characteristics of the EcoCAR's catalytic converter was first created. The oxygen storage behavior the catalyst is mainly dependent on the mass airflow into the engine and the air/fuel ratio of the exhaust gases before the catalyst. The catalytic converter model was optimized and then validated in the 2000 RPM operating region of the engine, which is the main operating region of the engine when the vehicle is in series mode. Once the catalytic converter model was validated, it could then be used in as the plant in the post-catalyst EGO sensor controller simulation. Although the simulation of the post-catalyst EGO sensor controller could not be experimentally validated during this research project it was still very useful to understanding the overall behavior of the controller.

The final step in this research was enabling the post-catalyst EGO sensor controller on the engine, and conducting emissions testing with the engine operating at steady state. The steady-state emissions data was then used to estimate the total emissions produced by the vehicle in series mode over the EPA's FTP-75 drive cycle. The results of the emissions test showed the EcoCAR vehicle can meet the EPA's Tier 2, Bin 5 emission regulations when the vehicle operates in series mode.

To conclude the post-catalyst EGO sensor controller research, a gain and set point schedule needs to be created for the EGO sensor controller. The emissions testing showed that the EGO sensor controller needed different combinations of the set point, proportional gain and integral gain, in order to minimize the emissions of the engine at different operating conditions. The discrepancy between the simulation and actual post-catalyst EGO sensor controller outputs should also be resolved, in order to validate the simulation of the EGO sensor controller. The engine also needs to be put through transient emission tests to ensure the engine can meet the EPA's Tier 2, Bin 5 emission regulations when the vehicle operates in parallel mode.

CHAPTER 8: BIBLIOGRAPHY

A. Selamet. “ME630: Lecture Notes 10.” 2 Nov. 2009.

Davis, Jonathan. “Development of an E85 Engine for the EcoCAR Challenge Hybrid Vehicle Competition.” Undergraduate Honors Thesis. Ohio State University (2010).

Erich P. Brandt, Y. Wang and Jesse W. Grizzle “Dynamic Modeling of a Three-Way Catalyst for SI Engine Exhaust Emission Control.” IEEE Transactions on Control Systems Technology, Vol 8.5, Sept. 2000.

Giovanni Fiengo, J.W. Grizzle, Jeffery A. Cook and Amey Y. Karnik “Dual-UEGO Active Catalyst Control for Emissions Reduction: Design and Experimental Validation.” IEEE Transactions on Control Systems Technology, Vol 13.5, Sept. 2005.

G. Holy, R. Bruck and P. Hirth “Improved Catalyst Systems for SULEV Legislation: First Practical Experience.” SAE Technical Paper No. 2000-01-0500.

Heywood, J. B. (1988). *Internal Combustion Engine Fundamentals*. McGraw-Hill, Inc.

J.G. Buglass, T.D.B. Morgan and J.O. Graupner “Interactions Between Exhaust Gas Composition and Oxygen Sensor Performance.” SAE Technical Paper No. 982646 (1998).

J. Schmidt, J. Franz, & N. Merdes “Utilization of Advanced Three-Way Catalyst Formulations on Ceramic Ultra Thin Wall Substrates for Future Legislation.” SAE International Paper No. 2002-01-0349.

Midlam-Mohler, Shawn. ME 631, Lecture 7. Winter 2010

Osamu Watanabe, Susumu Nakajima, Hiroyuki Goto and Toshibide Matsunaga “Development of CNG Engine with Variable Valve Timing Electronic Control.” SAE Technical Paper 2007-01-3615.

U.S. Environmental Protection Agency. *Emission Standards Reference Guide*. U.S. Environmental Protection Agency, 26 Oct. 2010. Web. 26 May 2010.

Wen Dai, Sreeni Cheemalamarri, Eric W. Curtis, Riadh Boussarsar and Richard K. Morton “Engine Cycle Simulation of Ethanol and Gasoline Blends.” SAE Technical Paper No. 2003-01-3093.

APPENDIX A

Specifications for the Electrically Heated Catalyst

A-Muster
A-Sample

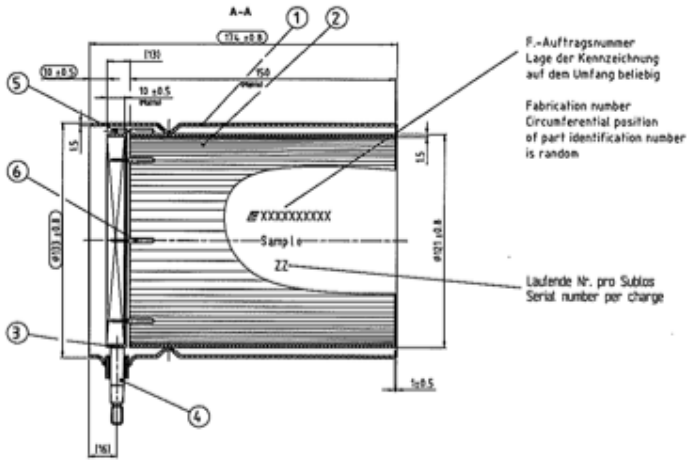

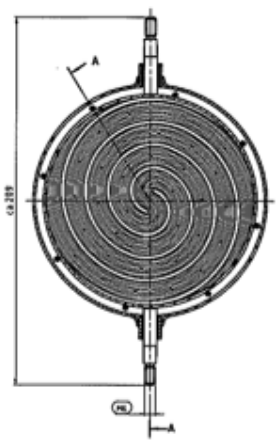

Pos.	Stck.	Benennung	Typ	Zeichng-Nr.
		Datenblatt für Heizkatmatrix		
		Verbind. Stützkat u. Halbschalen		S24090.01
6	37	Heizleiterabstützungen	D	S24324.04
5	8	Halteelemente		S24858.00
4	2	elektr. Durchführung		S24743.03
3	2	Halbschale f. Heizkatmatrix	D	S24917.01
2	1	Stützkatalysator	J	600186.00
1	1	Heizkatalysator-Mantel	J	S24915.01

Kontrollmaße
Dimensions to be checked

Matrix Heizscheibe/Heizkat-element		Matrix Stützkat/support-catalyst	Mantel / Mantle
Material	W.Nr./ 1.4767(med)	W.Nr./ 1.4767(med)	W.Nr./ 1.4509
Dicke / Thickness	0.05mm ±0.005 mm	0.04 mm ±0.005 mm	
Zelldichte / Cell density	400 cpsi	400 cpsi	
Wicklung / Winding	S-Form	S-Form	
Hohlvolumen / Hornet volume	1736 ml		
Gesamtgewicht / Weight total	(Referenzwert)		
elektr. Widerstand / electrical resistance	0.88 Ω±5%		

aktueller Status : Freigegeben Freigabe: Hepperger/ 10.08.2005
Dokument wurde EDV-technisch erzeugt und autorisiert.
Unterschrift ist nicht erforderlich.
Ausdruck unterliegt nicht dem Änderungsdienst.

Rev.	Datum Date	gezeichnet drawn	Kontrolliert prüfg. by	geprüft checked	Änderungsgrund / Reason Notice
gezeichnet drawn	03.08.05	Tschischka	F3-K		
kontrolliert prüfg. by					
geprüft checked					
Rel.-Ltg. Dept.					

Emicat Serie 6d
Ø118x10 +150 mm
400 cpsi + 400 cpsi R0.88 Ohm

Ident-Nr./No.
609520.00

EMITEC GmbH, Hauptstr. 128, 53797 Lohmar